Coupled electro-elastic analysis of functionally graded piezoelectric material plates

Chih-Ping Wu[*] and Shuang Ding

Department of Civil Engineering, National Cheng Kung University, Tainan 70101, Taiwan, ROC

Abstract. A unified formulation of finite layer methods (FLMs), based on the Reissner mixed variational theorem (RMVT), is developed for the three-dimensional (3D) coupled electro-elastic analysis of simply-supported, functionally graded piezoelectric material (FGPM) plates with open- and closed-circuit surface conditions and under electro-mechanical loads. In this formulation, the material properties of the plate are assumed to obey an exponent-law varying exponentially through the thickness coordinate, and the plate is divided into a number of finite rectangular layers, in which the trigonometric functions and Lagrange polynomials are used to interpolate the in- and out-of-plane variations of the primary field variables of each individual layer, respectively, such as the elastic displacement, transverse shear and normal stress, electric potential, and normal electric displacement components. The relevant orders used for expanding these variables in the thickness coordinate can be freely chosen as the linear, quadratic and cubic orders. Four different mechanical/electrical loading conditions applied on the top and bottom surfaces of the plate are considered, and the corresponding coupled electro-elastic analysis of the loaded FGPM plates is undertaken. The accuracy and convergence rate of the RMVT-based FLMs are assessed by comparing their solutions with the exact 3D piezoelectricity ones available in the literature.

Keywords: three-dimensional analysis; coupled electro-elastic analysis; static; finite layer methods; functionally graded materials; piezoelectric plates

1. Introduction

In recent decades, piezoelectric materials have been widely used to produce some beam-, plate- and shell-like smart structures with the advanced engineering applications for the purposes of sensing, actuating and controlling, due to their direct and converse effects, which means that a mechanical load applied to such structures will induce changes in the electric field variables of the structures, and vice versa. Many reports have examined conventional laminated piezoelectric structures, the material properties of which mismatch at the interfaces between adjacent layers, with reports indicating that in practical applications a number of weakness occur at these loactions, such as delamination, transverse matrix cracking, and huge residual thermo-mechanical stresses (Kashtalyan and Menshykova 2009, Woodward and Kashtalyan 2010). A new class of smart structures, called functionally graded piezoelectric material (FGPM) structures, the material properties of which continuously and gradually vary through the thickness coordinate, has thus

---

∗Corresponding author, Professor, E-mail: cpwu@mail.ncku.edu.tw

been developed to overcome these drawbacks. The coupled analysis of FGPM structures has since attracted considerable attention with the aims of both improving their working performances and enhancing their lifetime.

Based on the three-dimensional (3D) piezoelectricity theory, some exact solutions for the bending, vibration and buckling analyses of simply-supported, FGPM plates/shells have been presented to assess the accuracy and convergence rates of various related two-dimensional (2D) and approximate 3D theories. Pan (2003) and Pan and Han (2005) undertook the exact 3D analyses of simply-supported, functionally graded (FG) elastic plates and FG magneto-electro-elastic plates using the pseudo-Stroh formalism (PSF), in which the material properties were assumed to vary exponentially in the thickness coordinate, and the effect of the material-property gradient index on the induced deformations and stresses was examined. The PSF was further extended to the cylindrical bending analysis of simply-supported, FGPM laminates by Lu *et al*. (2005, 2006). Zhong and Shang (2003) and Zhong and Yu (2006) investigated the static behaviors and the free and forced vibration of FGPM plates with fully simple supports on the basis of the state space method. Arefi *et al*. (2012) presented the analytical solutions of an FGPM cylinder in a magnetic field and under elasto-thermo-electric loads, in which the material properties, except for the Poisson's ratio, were assumed to vary continuously and gradually along the thickness coordinate based on a power function. Using the Airy stress function method with plane strain assumptions, Zhang and Shi (2010) obtained the exact solutions of FGPM cylinders with different piezoelectric parameters and the lateral surfaces of the cylinders subjected to electric potential and mechanical loads. Wu and Syu (2007) and Wu and Tsai (2007) studied the static behaviors of FGPM cylindrical shells and FG magneto-electro-elastic doubly-curved ones using the perturbation method, and their free vibration counterparts were examined by Tsai and Wu (2008) and Wu and Tsai (2009) using the method of multiple time scales. Comprehensive literature surveys related to the 3D analytical and 2D numerical approaches for the analysis of multilayered piezoelectric plates/shells and FGPM ones were conducted by Saravanos and Heyliger (1999), Tang *et al*. (1996) and Wu *et al*. (2008).

In order to extend the scope of the coupled electro-elastic analyses of FGPM structures, a number of numerical methods combining 2D and 3D theories have been presented, such as the finite element (FE), finite strip and meshless approaches. Wu *et al*. (2002) developed a higher-order theory for the analysis of FGPM cylindrical shells under electro-mechanical loads, in which the sensing and actuating behaviors of the shells were examined. Loja *et al*. (2013) studied the static behaviors and free vibration responses of sandwich FGM plates with the surface-bonding piezoelectric sensor and actuator layers using B-spline finite strip models based on a variety of first- and higher-order shear deformation theories (FSDTs and HSDTs). In conjunction with the energy method and FSDT, Arefi and Rahimi (2014) carried out 2D electro-elastic analysis of an FGPM cylinder under internal pressure, in which the effects of a local support on the distributions of elastic and electric variables were evaluated. Arefi (2014) developed a generalized shear deformation theory for the thermo-mechanical analysis of FGM cylindrical shells subjected to the external loads. Ootao and Ishihara (2013) presented the exact solution for the transient thermal stress analysis of FGM hollow cylinders with the material properties of a piecewise power law. Sladek *et al*. (2010, 2012, 2013) proposed a meshless local Petrov-Galerkin method for the bending analysis of FGPM circular plates and laminated composite ones bounded with the piezoelectric sensors and actuators on the lateral surfaces, in which the shape functions of electric and elastic variables were constructed using the moving least square method. Based on the FSDT, Liew *et al*. (2003a, b) developed a finite element formulation for the static and dynamic analyses

of FGM plates, in which the material properties were assumed to obey a power-law distribution of the volume fractions of the constituents through the thickness coordinate. Some control algorithms coupling the direct and converse piezoelectric effects are also applied in the literature to provide feedback control of the integrated FGM plates. Carrera (2003) proposed a compact and generalized formulation, called Carrera's unified formulation (CUF), for the bending, vibration and buckling analyses of laminated composite plates and shells, in which the order of each field variable expanded in the thickness coordinate remains the same, and can be freely chosen, and the stiffness matrices of all possible theories were generated from the expansion of the fundamental nuclei, which is a three-by-three matrix. A number of 2D refined and advanced theories based on the principle of virtual displacement (PVD) and Reissner's mixed variational theorem (RMVT) (Reissner 1984, 1986) can be thus included as special cases of the CUF. Finally, the CUF has been successfully extended to the analyses of FGM plates and shells by Brischetto and Carrera (2010, 2012), and to those of laminated piezoelectric plates and shells by Ballhause *et al.* (2005), Carrera and Boscolo (2007) and Carrera *et al.* (2008, 2010).

Based on the RMVT, Wu and Li (2010 a, b), Wu and Chang (2012) and Wu *et al.* (2014) developed the unified formulations of finite layer methods (FLMs) for the 3D static and vibration analyses of simply-supported, multilayered FG elastic plates/cylinders and laminated composite ones. Subsequently, Wu and Li (2013a, b) developed the RMVT-based finite rectangular and cylindrical prism methods (FRPMs and FCPMs) for the 3D bending analysis of the above-mentioned structures with various boundary conditions and under mechanical loads. In the implementations of these FLMs, the results are shown to be in excellent agreement with the exact 3D elasticity solutions available in the literature, with a fast convergence rate. In this article, the formulations of RMVT-based FLMs for the elastic structures were thus extended to the coupled electro-elastic analysis of single- and multi-layered FGPM plates with open- and closed-circuit surface conditions and under electro-mechanical loads. The relevant orders used for expanding the electric and elastic variables through the thickness coordinate can be freely chosen as linear, quadratic and cubic orders, and the accuracy and convergence rate of various FLMs are examined by comparing their solutions with the exact 3D piezoelectricity ones available in the literature. The material properties of the plate are assumed to obey an exponent-law varying exponentially through the thickness coordinate, and four different electric and mechanical loading conditions applied on the lateral surfaces are considered. A parametric study related to the influence of various factors on the coupled electro-elastic behaviors of the FGPM plate is carried out, such as the material-property gradient index, different surface conditions and aspect ratios.

2. RMVT-based FLMs

In this article, we consider a simply-supported, FGPM plate with the open- and closed-circuit surface conditions, and subjected to electro-mechanical loads on the top and bottom surfaces, as shown in Fig. 1(a), in which the plate is artificially divided into a number of rectangular layers. A Cartesian global coordinate system (i.e., x, y and ζ coordinates) is located on the middle plane of the plate, and a set of Cartesian local thickness coordinates, z_m ($m = 1, 2, 3, \cdots, N_l$), is located at the mid-plane of each divided layer, as shown in Fig. 1(b), in which N_l is the total number of the layers constituting the plate. The thicknesses of each individual layer and the plate are

h_m $(m = 1, 2, \cdots, N_l)$ and h, respectively, while $h = \sum_{m=1}^{N_l} h_m$. L_x and L_y denote the in-plane dimensions in the x and y directions, respectively. The relationship between the global and local thickness coordinates in the mth-layer is $\zeta = \bar{\zeta}_m + z_m$, in which $\bar{\zeta}_m = (\zeta_m + \zeta_{m-1})/2$, and ζ_m and ζ_{m-1} are the global thickness coordinates measured from the mid-plane of the plate to the top and bottom surfaces of the mth-layer, respectively.

2.1 Generalized Kinematic and Kinetic assumptions

A unified formulation of RMVT-based FLMs is developed for the 3D coupled electro-elastic analysis of N_l-layered FGPM plates subjected to electro-mechanical loads. The elastic displacement and electric potential components of a typical layer (i.e., the mth-layer) of the plate, of which the domains are in $0 \le x \le L_x$, $0 \le y \le L_y$ and $(-h_m/2) \le z_m \le (h_m/2)$, are given by
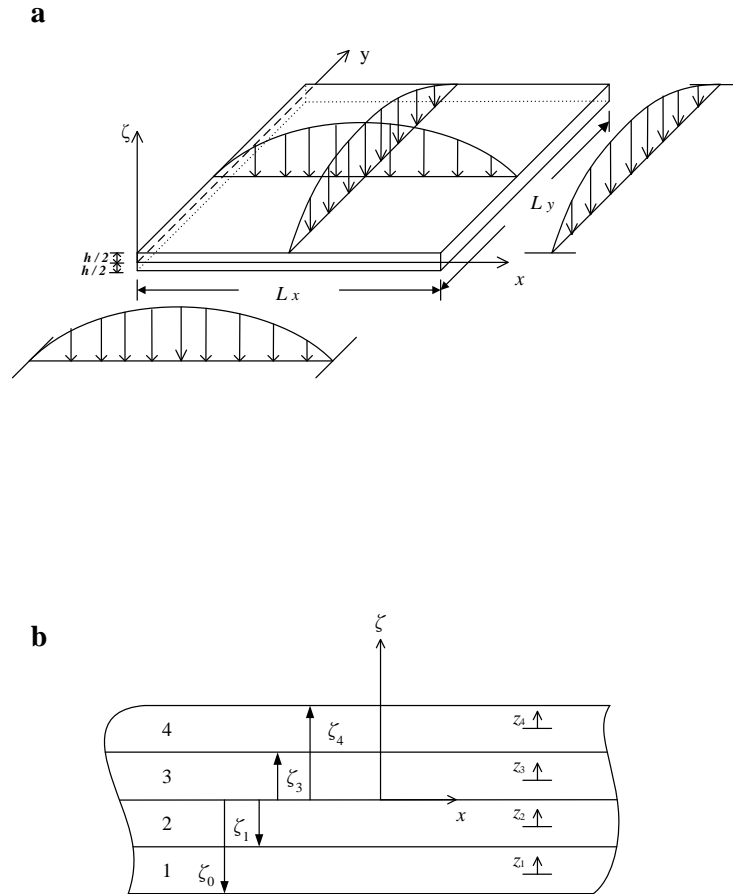
a

b

Fig. 1 (a) The configuration and loading conditions of an FGPM plate. (b) The global and local coordinates of the plate, in which $N_l = 4$

$$u_x^{(m)}(x, y, z_m) = \sum_{i=1}^{n_u+1} \left[\psi_u^{(m)}(z_m)\right]_i \left[u^{(m)}(x, y)\right]_i \tag{1}$$

$$u_y^{(m)}(x, y, z_m) = \sum_{i=1}^{n_u+1} \left[\psi_u^{(m)}(z_m)\right]_i \left[v^{(m)}(x, y)\right]_i \tag{2}$$

$$u_\zeta^{(m)}(x, y, z_m) = \sum_{i=1}^{n_w+1} \left[\psi_w^{(m)}(z_m)\right]_i \left[w^{(m)}(x, y)\right]_i \tag{3}$$

$$\Phi^{(m)}(x, y, z_m) = \sum_{i=1}^{n_\phi+1} \left[\psi_\phi^{(m)}(z_m)\right]_i \left[\phi^{(m)}(x, y)\right]_i \tag{4}$$

where $u_x^{(m)}$, $u_y^{(m)}$ and $u_\zeta^{(m)}$ denote the elastic displacement components of the mth-layer of the plate in the x, y and ζ directions, respectively, and $\Phi^{(m)}$ is the electric potential of the mth-layer of the plate; $\left(u^{(m)}\right)_i$, $\left(v^{(m)}\right)_i$, $\left(w^{(m)}\right)_i$ and $\left(\phi^{(m)}\right)_i$ are the elastic displacement and electric potential components at the ith-nodal plane of the mth-layer of the plate; and $\left(\psi_u^{(m)}\right)_i$, $\left(\psi_w^{(m)}\right)_i$ and $\left(\psi_\phi^{(m)}\right)_i$ are the corresponding shape functions; n_u, n_w and n_ϕ denote the related orders used for the expansion of the in- and out-of-plane displacement and electric potential components, respectively.

The transverse shear and normal stress components, and the normal electric displacement one, are also regarded as the primary variables in these RMVT-based FLMs, and are assumed as follows

$$\tau_{x\zeta}^{(m)}(x, y, z_m) = \sum_{i=1}^{n_\tau+1} \left[\psi_\tau^{(m)}(z_m)\right]_i \left[\tau_{13}^{(m)}(x, y)\right]_i \tag{5}$$

$$\tau_{y\zeta}^{(m)}(x, y, z_m) = \sum_{i=1}^{n_\tau+1} \left[\psi_\tau^{(m)}(z_m)\right]_i \left[\tau_{23}^{(m)}(x, y)\right]_i \tag{6}$$

$$\sigma_\zeta^{(m)}(x, y, z_m) = \sum_{i=1}^{n_\sigma+1} \left[\psi_\sigma^{(m)}(z_m)\right]_i \left[\sigma_3^{(m)}(x, y)\right]_i \tag{7}$$

$$D_\zeta^{(m)}(x, y, z_m) = \sum_{i=1}^{n_d+1} \left[\psi_d^{(m)}(z_m)\right]_i \left[D_3^{(m)}(x, y)\right]_i \tag{8}$$

where $\left(\tau_{13}^{(m)}\right)_i$, $\left(\tau_{23}^{(m)}\right)_i$, $\left(\sigma_3^{(m)}\right)_i$ and $\left(D_3^{(m)}\right)_i$ are the transverse shear and normal stress components and the normal electric displacement one at the ith-nodal plane of the mth-layer of the plate; $\left(\psi_\tau^{(m)}\right)_i$, $\left(\psi_\sigma^{(m)}\right)_i$ and $\left(\psi_d^{(m)}\right)_i$ are the corresponding shape functions; n_τ, n_σ and n_d denote the related orders used for the expansion of the transverse shear and normal stress, and normal electric displacement components, respectively.

For a typical layer, the linear constitutive equations, which are valid for the orthotropic piezoelectric materials, are given by

$$
\begin{Bmatrix} \sigma_x^{(m)} \\ \sigma_y^{(m)} \\ \sigma_\zeta^{(m)} \\ \tau_{y\zeta}^{(m)} \\ \tau_{x\zeta}^{(m)} \\ \tau_{xy}^{(m)} \end{Bmatrix} = \begin{bmatrix} c_{11}^{(m)} & c_{12}^{(m)} & c_{13}^{(m)} & 0 & 0 & 0 \\ c_{12}^{(m)} & c_{22}^{(m)} & c_{23}^{(m)} & 0 & 0 & 0 \\ c_{13}^{(m)} & c_{23}^{(m)} & c_{33}^{(m)} & 0 & 0 & 0 \\ 0 & 0 & 0 & c_{44}^{(m)} & 0 & 0 \\ 0 & 0 & 0 & 0 & c_{55}^{(m)} & 0 \\ 0 & 0 & 0 & 0 & 0 & c_{66}^{(m)} \end{bmatrix} \begin{Bmatrix} \varepsilon_x^{(m)} \\ \varepsilon_y^{(m)} \\ \varepsilon_\zeta^{(m)} \\ \gamma_{y\zeta}^{(m)} \\ \gamma_{x\zeta}^{(m)} \\ \gamma_{xy}^{(m)} \end{Bmatrix} - \begin{bmatrix} 0 & 0 & e_{31}^{(m)} \\ 0 & 0 & e_{32}^{(m)} \\ 0 & 0 & e_{33}^{(m)} \\ 0 & e_{24}^{(m)} & 0 \\ e_{15}^{(m)} & 0 & 0 \\ 0 & 0 & 0 \end{bmatrix} \begin{bmatrix} E_x^{(m)} \\ E_y^{(m)} \\ E_\zeta^{(m)} \end{bmatrix} \tag{9}
$$

$$
\begin{Bmatrix} D_x^{(m)} \\ D_y^{(m)} \\ D_\zeta^{(m)} \end{Bmatrix} = \begin{bmatrix} 0 & 0 & 0 & 0 & e_{15}^{(m)} & 0 \\ 0 & 0 & 0 & e_{24}^{(m)} & 0 & 0 \\ e_{31}^{(m)} & e_{32}^{(m)} & e_{33}^{(m)} & 0 & 0 & 0 \end{bmatrix} \begin{Bmatrix} \varepsilon_x^{(m)} \\ \varepsilon_y^{(m)} \\ \varepsilon_\zeta^{(m)} \\ \gamma_{y\zeta}^{(m)} \\ \gamma_{x\zeta}^{(m)} \\ \gamma_{xy}^{(m)} \end{Bmatrix} + \begin{bmatrix} \eta_{11}^{(m)} & 0 & 0 \\ 0 & \eta_{22}^{(m)} & 0 \\ 0 & 0 & \eta_{33}^{(m)} \end{bmatrix} \begin{bmatrix} E_x^{(m)} \\ E_y^{(m)} \\ E_\zeta^{(m)} \end{bmatrix} \tag{10}
$$

where $\sigma_x^{(m)}$, $\sigma_y^{(m)}, \cdots$, and $\tau_{xy}^{(m)}$ are the stress components; $\varepsilon_x^{(m)}$, $\varepsilon_y^{(m)}, \cdots$, and $\gamma_{xy}^{(m)}$ are the strain components; $D_x^{(m)}$, $D_y^{(m)}$ and $D_\zeta^{(m)}$ are the electric displacement components; $E_x^{(m)}$, $E_y^{(m)}$ and $E_\zeta^{(m)}$ are the electric field components; $c_{ij}^{(m)}$, $e_{kl}^{(m)}$ and $\eta_{ll}^{(m)}$ are the elastic, piezoelectric and dielectric permeability coefficients, respectively, which are variable through the thickness coordinate in the FGPM plate.

The strain-displacement relations for each individual layer are written as follows

$$
\varepsilon_x^{(m)} = u_x^{(m)}{}_{,x} = \sum_{i=1}^{n_u+1} \left(\psi_u^{(m)} \right)_i u_i^{(m)}{}_{,x} \tag{11}
$$

$$
\varepsilon_y^{(m)} = u_y^{(m)}{}_{,y} = \sum_{i=1}^{n_u+1} \left(\psi_u^{(m)} \right)_i v_i^{(m)}{}_{,y} \tag{12}
$$

$$
\varepsilon_\zeta^{(m)} = u_\zeta^{(m)}{}_{,\zeta} = \sum_{i=1}^{n_w+1} D\left(\psi_w^{(m)} \right)_i w_i^{(m)} \tag{13}
$$

$$
\gamma_{x\zeta}^{(m)} = u_x^{(m)}{}_{,\zeta} + u_\zeta^{(m)}{}_{,x} = \sum_{i=1}^{n_u+1} D\left(\psi_u^{(m)} \right)_i u_i^{(m)} + \sum_{i=1}^{n_w+1} \left(\psi_w^{(m)} \right)_i w_i^{(m)}{}_{,x} \tag{14}
$$

$$
\gamma_{y\zeta}^{(m)} = u_y^{(m)}{}_{,\zeta} + u_\zeta^{(m)}{}_{,y} = \sum_{i=1}^{n_u+1} D\left(\psi_u^{(m)} \right)_i v_i^{(m)} + \sum_{i=1}^{n_w+1} \left(\psi_w^{(m)} \right)_i w_i^{(m)}{}_{,y} \tag{15}
$$

$$
\gamma_{xy}^{(m)} = u_x^{(m)}{}_{,y} + u_y^{(m)}{}_{,x} = \sum_{i=1}^{n_u+1} \left(\psi_u^{(m)} \right)_i u_i^{(m)}{}_{,y} + \sum_{i=1}^{n_u+1} \left(\psi_u^{(m)} \right)_i v_i^{(m)}{}_{,x} \tag{16}
$$

where the commas denote partial differentiation with respect to the suffix variables; and $D\left(\psi_j^{(m)} \right)_i = d\left(\psi_j^{(m)} \right)_i / dz_m$ .in which $j = u$ and w.

The electric field-electric potential relations for each individual layer are given by

$$E_x^{(m)} = \Phi^{(m)},_x = \sum_{i=1}^{n_\varphi+1} \left(\psi_\varphi^{(m)}\right)_i \varphi_i^{(m)},_x \tag{17}$$

$$E_y^{(m)} = \Phi^{(m)},_y = \sum_{i=1}^{n_\varphi+1} \left(\psi_\varphi^{(m)}\right)_i \varphi_i^{(m)},_y \tag{18}$$

$$E_\zeta^{(m)} = \Phi^{(m)},_\zeta = \sum_{i=1}^{n_\varphi+1} D\left(\psi_\varphi^{(m)}\right)_i \varphi_i^{(m)} \tag{19}$$

2.2 The Reissner mixed variational theorem

The Reissner mixed variational theorem is used to derive the Euler-Lagrange equations of the plate for RMVT-based FLMs, and its corresponding energy functional for the plate is written in the form of

$$\begin{aligned}
\Pi_R &= \int_{-h/2}^{h/2} \iint_\Omega \left[\sigma_x \varepsilon_x + \sigma_y \varepsilon_y + \sigma_\zeta \varepsilon_\zeta + \tau_{x\zeta}\gamma_{x\zeta} + \tau_{y\zeta}\gamma_{y\zeta} + \tau_{xy}\gamma_{xy} - D_x E_x - D_y E_y - D_\zeta E_\zeta - B(\sigma_{ij}, D_k)\right] dx\,dy\,d\zeta \\
&\quad - \iint_{\Omega_\sigma^\pm} \overline{q}_\zeta^\pm(x,\,y)\, u_\zeta^\pm\, dx\,dy - \iint_{\Omega_{\overline{D}}^\pm} \overline{D}_\zeta^\pm(x,\,y)\, \Phi^\pm\, dx\,dy - \iint_{\Omega_\Phi^\pm} D_\zeta\left(\Phi - \overline{\Phi}^\pm\right) dx\,dy \\
&\quad - \int_{-h/2}^{h/2} \int_{\Gamma_\sigma} \left(\overline{t}_x\, u_x + \overline{t}_y\, u_y + \overline{t}_\zeta\, u_\zeta\right) d\Gamma\, d\zeta - \int_{-h/2}^{h/2} \int_{\Gamma_D} \left(\overline{D}_n\, \Phi\right) d\Gamma\, d\zeta \\
&\quad - \int_{-h/2}^{h/2} \int_{\Gamma_u} \left[(u_x - \overline{u}_x)\,t_x + (u_y - \overline{u}_y)\,t_y + (u_\zeta - \overline{u}_\zeta)\,t_\zeta\right] d\Gamma\, d\zeta - \int_{-h/2}^{h/2} \int_{\Gamma_\Phi} D_n\left(\Phi - \overline{\Phi}\right) d\Gamma\, d\zeta,
\end{aligned} \tag{20}$$

where Ω denotes the plate domain on the $x-y$ plane, and $\Omega^\pm$ denotes the top surface ($\zeta = h/2$) and the bottom one ($\zeta = -h/2$) of the plate, in which the transverse load ($\overline{q}_\zeta^\pm$), electric potential ($\overline{\Phi}^\pm$) or normal electric displacement ($\overline{D}_\zeta^\pm$) are applied; Γ_σ, Γ_u, Γ_D and Γ_Φ denote the portions of the edge boundary, where the surface traction, elastic displacement, electric potential and normal electric displacement components are prescribed, respectively (i.e., $t_i = \overline{t}_i$ and $u_i = \overline{u}_i$, in which $i = x$, y and ζ; $\Phi = \overline{\Phi}$; $D_n = \overline{D}_n$); $B(\sigma_{ij}, D_k)$ is the complementary energy density function.

In the formulation, we take the elastic displacement, transverse shear and normal stress, electric potential and normal electric displacement components to be the primary variables subject to variation. Using the generalized kinematic and kinetic assumptions given in Eqs. (1)-(8), we may express the first-order variation of the Reissner energy functional as follows

$$\delta\Pi_R = \iint_\Omega \sum_{m=1}^{N_l} \int_{-h_m/2}^{h_m/2} \left\{ \left(\delta\boldsymbol{\varepsilon}_p^{(m)}\right)^T \boldsymbol{\sigma}_p^{(m)} + \left(\delta\boldsymbol{\varepsilon}_s^{(m)}\right)^T \boldsymbol{\sigma}_s^{(m)} + \delta\varepsilon_\zeta^{(m)} \sigma_\zeta^{(m)} + \left(\delta\boldsymbol{\sigma}_s^{(m)}\right)^T \left(\boldsymbol{\varepsilon}_s^{(m)} - \mathbf{S}_\sigma^{(m)} \boldsymbol{\sigma}_s^{(m)} - \mathbf{S}_e^{(m)} \mathbf{E}_s^{(m)}\right) \right.$$

$$+ \delta\sigma_\zeta^{(m)} \left[\varepsilon_\zeta^{(m)} - \overline{\eta}^{(m)} \sigma_\zeta^{(m)} + \left(\mathbf{Q}_a^{(m)}\right)^T \boldsymbol{\varepsilon}_p^{(m)} - \overline{e}^{(m)} D_\zeta^{(m)}\right] - \left(\delta\mathbf{E}_s^{(m)}\right)^T \mathbf{D}_s^{(m)} - \delta E_\zeta^{(m)} D_\zeta^{(m)}$$

$$\left. - \delta D_\zeta^{(m)} \left[E_\zeta^{(m)} + \overline{e}^{(m)} \sigma_\zeta^{(m)} - \left(\mathbf{Q}_b^{(m)}\right)^T \boldsymbol{\varepsilon}_p^{(m)} - \overline{c}^{(m)} D_\zeta^{(m)}\right] \right\} dx\, dy\, dz_m \tag{21}$$

$$- \iint_{\Omega_\sigma^\pm} \overline{q}_\zeta^\pm(x,\,y)\, \delta u_\zeta^\pm\, dx dy - \iint_{\Omega_D^\pm} \overline{D}_\zeta^\pm(x,\,y)\, \delta\Phi^\pm\, dx dy - \iint_{\Omega_D^\pm} (\Phi^\pm - \overline{\Phi}^\pm)\, \delta\overline{D}_\zeta^\pm\, dx dy$$

$$- \int_{-h/2}^{h/2} \int_{\Gamma_\sigma} \left(\overline{t}_x\, \delta u_x + \overline{t}_y\, \delta u_y + \overline{t}_\zeta\, \delta u_\zeta\right) d\Gamma\, d\zeta - \int_{-h/2}^{h/2} \int_{\Gamma_D} \left(\overline{D}_n\, \delta\Phi\right) d\Gamma\, d\zeta - \int_{-h/2}^{h/2} \int_{\Gamma_\phi} (\Phi - \overline{\Phi})\, \delta D_n d\Gamma\, d\zeta$$

$$- \int_{-h/2}^{h/2} \int_{\Gamma_u} \left[(u_x - \overline{u}_x)\, \delta t_x + (u_y - \overline{u}_y)\, \delta t_y + (u_\zeta - \overline{u}_\zeta)\, \delta t_\zeta\right] d\Gamma\, d\zeta,$$

where the superscript of T denotes the transposition of the matrices or vectors; and Γ_u and Γ_σ stand for the boundary edges, in which the essential and natural conditions are prescribed.

$$\boldsymbol{\varepsilon}_p^{(m)} = \begin{bmatrix} \varepsilon_x^{(m)} & \varepsilon_y^{(m)} & \gamma_{xy}^{(m)} \end{bmatrix}^T = \mathbf{B}_1^{(m)} \mathbf{u}^{(m)}, \qquad \boldsymbol{\varepsilon}_s^{(m)} = \begin{bmatrix} \gamma_{x\zeta}^{(m)} & \gamma_{y\zeta}^{(m)} \end{bmatrix}^T = \mathbf{B}_3^{(m)} \mathbf{u}^{(m)} + \mathbf{B}_4^{(m)} \mathbf{w}^{(m)},$$

$$\varepsilon_\zeta^{(m)} = \mathbf{B}_6^{(m)} \mathbf{w}^{(m)}, \qquad \boldsymbol{\sigma}_p^{(m)} = \begin{bmatrix} \sigma_x^{(m)} & \sigma_y^{(m)} & \tau_{xy}^{(m)} \end{bmatrix}^T = \mathbf{Q}_p^{(m)} \mathbf{B}_1^{(m)} \mathbf{u}^{(m)} + \mathbf{Q}_a^{(m)} \mathbf{B}_2^{(m)} \boldsymbol{\sigma}^{(m)} + \mathbf{Q}_b^{(m)} \mathbf{B}_9^{(m)} \mathbf{D}^{(m)},$$

$$\boldsymbol{\sigma}_s^{(m)} = \begin{bmatrix} \tau_{x\zeta}^{(m)} & \tau_{y\zeta}^{(m)} \end{bmatrix}^T = \mathbf{B}_5^{(m)} \boldsymbol{\tau}^{(m)}, \qquad \sigma_\zeta^{(m)} = \mathbf{B}_2^{(m)} \boldsymbol{\sigma}^{(m)}, \qquad \mathbf{E}_s^{(m)} = \begin{bmatrix} E_x^{(m)} & E_y^{(m)} \end{bmatrix}^T = -\mathbf{B}_7^{(m)} \boldsymbol{\Phi}^{(m)},$$

$$E_\zeta^{(m)} = -\mathbf{B}_8^{(m)} \boldsymbol{\Phi}^{(m)}, \qquad \mathbf{D}_s^{(m)} = \begin{bmatrix} D_x^{(m)} & D_y^{(m)} \end{bmatrix}^T = \mathbf{S}_e^{(m)} \mathbf{B}_5^{(m)} \boldsymbol{\tau}^{(m)} + \mathbf{S}_\eta^{(m)} \mathbf{B}_7^{(m)} \boldsymbol{\Phi}^{(m)}, \qquad D_\zeta^{(m)} = \mathbf{B}_9^{(m)} \mathbf{D}^{(m)},$$

$$\mathbf{u}^{(m)} = \begin{bmatrix} u_i^{(m)} \\ v_i^{(m)} \end{bmatrix}_{i=1,2,\cdots,n_u+1}, \qquad \mathbf{w}^{(m)} = \begin{bmatrix} w_i^{(m)} \end{bmatrix}_{i=1,2,\cdots,n_w+1}, \qquad \boldsymbol{\tau}^{(m)} = \begin{bmatrix} \begin{pmatrix} \tau_{13}^{(m)} \end{pmatrix}_i \\ \begin{pmatrix} \tau_{23}^{(m)} \end{pmatrix}_i \end{bmatrix}_{i=1,2,\cdots,n_\tau+1}, \qquad \boldsymbol{\sigma}^{(m)} = \begin{bmatrix} \begin{pmatrix} \sigma_3^{(m)} \end{pmatrix}_i \end{bmatrix}_{i=1,2,\cdots,n_\sigma+1},$$

$$\boldsymbol{\Phi}^{(m)} = \begin{bmatrix} \Phi_i^{(m)} \end{bmatrix}_{i=1,2,\cdots,n_\phi+1}, \mathbf{D}^{(m)} = \begin{bmatrix} \begin{pmatrix} D_3^{(m)} \end{pmatrix}_i \end{bmatrix}_{i=1,2,\cdots,n_d+1}, \mathbf{S}_\sigma^{(m)} = \begin{bmatrix} \begin{pmatrix} 1/c_{55}^{(m)} \end{pmatrix} & 0 \\ 0 & \begin{pmatrix} 1/c_{44}^{(m)} \end{pmatrix} \end{bmatrix}, \mathbf{S}_e^{(m)} = \begin{bmatrix} \begin{pmatrix} e_{15}^{(m)}/c_{55}^{(m)} \end{pmatrix} & 0 \\ 0 & \begin{pmatrix} e_{24}^{(m)}/c_{44}^{(m)} \end{pmatrix} \end{bmatrix},$$

$$\mathbf{S}_\eta^{(m)} = \begin{bmatrix} \begin{pmatrix} \eta_{11}^{(m)} + e_{15}^{(m)} e_{15}^{(m)}/c_{55}^{(m)} \end{pmatrix} & 0 \\ 0 & \begin{pmatrix} \eta_{22}^{(m)} + e_{24}^{(m)} e_{24}^{(m)}/c_{44}^{(m)} \end{pmatrix} \end{bmatrix}, \qquad \mathbf{Q}_p^{(m)} = \begin{bmatrix} Q_{11}^{(m)} & Q_{12}^{(m)} & 0 \\ Q_{12}^{(m)} & Q_{22}^{(m)} & 0 \\ 0 & 0 & Q_{66}^{(m)} \end{bmatrix},$$

$$\mathbf{Q}_a^{(m)} = \begin{bmatrix} a_1^{(m)} \\ a_2^{(m)} \\ 0 \end{bmatrix}, \qquad \mathbf{Q}_b^{(m)} = \begin{bmatrix} b_1^{(m)} \\ b_2^{(m)} \\ 0 \end{bmatrix}, \qquad \mathbf{B}_1^{(m)} = \begin{bmatrix} \begin{pmatrix} \psi_u^{(m)} \end{pmatrix}_i \partial_x & 0 \\ 0 & \begin{pmatrix} \psi_u^{(m)} \end{pmatrix}_i \partial_y \\ \begin{pmatrix} \psi_u^{(m)} \end{pmatrix}_i \partial_y & \begin{pmatrix} \psi_u^{(m)} \end{pmatrix}_i \partial_x \end{bmatrix}_{i=1,2,\cdots,n_u+1},$$

$$\mathbf{B}_2^{(m)} = \begin{bmatrix} \begin{pmatrix} \psi_\sigma^{(m)} \end{pmatrix}_i \end{bmatrix}_{i=1,2,\cdots,n_\sigma+1}, \qquad \mathbf{B}_3^{(m)} = \begin{bmatrix} \begin{pmatrix} D\psi_u^{(m)} \end{pmatrix}_i & 0 \\ 0 & \begin{pmatrix} D\psi_u^{(m)} \end{pmatrix}_i \end{bmatrix}_{i=1,2,\cdots,n_u+1},$$

$$\mathbf{B}_4^{(m)} = \begin{bmatrix} \begin{pmatrix} \psi_w^{(m)} \end{pmatrix}_i \partial_x \\ \begin{pmatrix} \psi_w^{(m)} \end{pmatrix}_i \partial_y \end{bmatrix}_{i=1,2,\cdots,n_w+1}, \qquad \mathbf{B}_5^{(m)} = \begin{bmatrix} \begin{pmatrix} \psi_\tau^{(m)} \end{pmatrix}_i & 0 \\ 0 & \begin{pmatrix} \psi_\tau^{(m)} \end{pmatrix}_i \end{bmatrix}_{i=1,2,\cdots,n_\tau+1}, \qquad \mathbf{B}_6^{(m)} = \begin{bmatrix} \begin{pmatrix} D\psi_w^{(m)} \end{pmatrix}_i \end{bmatrix}_{i=1,2,\cdots,n_w+1},$$

$$\mathbf{B}_7^{(m)} = \begin{bmatrix} \left(\psi_\phi^{(m)}\right)_i \partial_x \\ \left(\psi_\phi^{(m)}\right)_i \partial_y \end{bmatrix}_{i=1,2,\cdots,n_\phi+1}, \qquad \mathbf{B}_8^{(m)} = \left[D\left(\psi_\phi^{(m)}\right)_i \right]_{i=1,2,\cdots,n_\phi+1}, \qquad \mathbf{B}_9^{(m)} = \left[\left(\psi_d^{(m)}\right)_i \right]_{i=1,2,\cdots,n_d+1},$$

$$Q_{ij}^{(m)} = c_{ij}^{(m)} - a_j^{(m)} c_{i3}^{(m)} - b_j^{(m)} e_{3i}^{(m)}, \qquad Q_{66}^{(m)} = c_{66}^{(m)},$$

$$a_i^{(m)} = \left(\eta_{33}^{(m)} c_{i3}^{(m)} + e_{33}^{(m)} e_{3i}^{(m)}\right)/\left(\eta_{33}^{(m)} c_{33}^{(m)} + e_{33}^{(m)} e_{33}^{(m)}\right), \qquad b_i^{(m)} = \left(e_{33}^{(m)} c_{i3}^{(m)} - e_{3i}^{(m)} c_{33}^{(m)}\right)/\left(\eta_{33}^{(m)} c_{33}^{(m)} + e_{33}^{(m)} e_{33}^{(m)}\right),$$

$$\bar{c}^{(m)} = c_{33}^{(m)}/\left(\eta_{33}^{(m)} c_{33}^{(m)} + e_{33}^{(m)} e_{33}^{(m)}\right), \qquad \bar{e}^{(m)} = e_{33}^{(m)}/\left(\eta_{33}^{(m)} c_{33}^{(m)} + e_{33}^{(m)} e_{33}^{(m)}\right), \qquad \bar{\eta}^{(m)} = \eta_{33}^{(m)}/\left(\eta_{33}^{(m)} c_{33}^{(m)} + e_{33}^{(m)} e_{33}^{(m)}\right).$$

2.3 Euler–lagrange equations

The static behaviors of simply-supported, single- and multi-layered functionally graded piezoelectric plates under electro-mechanical loads are studied in the following illustrative examples. The applied loading conditions on the lateral surfaces of the plate are prescribed as follows:

Case 1. Closed-circuit surface conditions on which the mechanical loads are applied,

$$\left[\tau_{x\zeta}^{(N_l)}(x,y,h/2) \quad \tau_{y\zeta}^{(N_l)}(x,y,h/2) \quad \sigma_\zeta^{(N_l)}(x,y,h/2) \quad \Phi^{(N_l)}(x,y,h/2)\right] = \left[0 \quad 0 \quad \bar{q}_\zeta^+(x,y) \quad 0\right] \text{ on the top surface, (22a)}$$

$$\left[\tau_{x\zeta}^{(1)}(x,y,-h/2) \quad \tau_{y\zeta}^{(1)}(x,y,-h/2) \quad \sigma_\zeta^{(1)}(x,y,-h/2) \quad \Phi^{(1)}(x,y,-h/2)\right] = \left[0 \quad 0 \quad 0 \quad 0\right], \text{ on the bottomn surface;(22b)}$$

Case 2. Closed-circuit surface conditions on which the electric potentials are applied,

$$\left[\tau_{x\zeta}^{(N_l)}(x,y,h/2) \quad \tau_{y\zeta}^{(N_l)}(x,y,h/2) \quad \sigma_\zeta^{(N_l)}(x,y,h/2) \quad \Phi^{(N_l)}(x,y,h/2)\right] = \left[0 \quad 0 \quad 0 \quad \bar{\Phi}^+(x,y)\right] \text{ on the top surface, (23a)}$$

$$\left[\tau_{x\zeta}^{(1)}(x,y,-h/2) \quad \tau_{y\zeta}^{(1)}(x,y,-h/2) \quad \sigma_\zeta^{(1)}(x,y,-h/2) \quad \Phi^{(1)}(x,y,-h/2)\right] = \left[0 \quad 0 \quad 0 \quad 0\right], \text{ on the bottom surface; (23b)}$$

Case 3. Open-circuit surface conditions on which the mechanical loads are applied,

$$\left[\tau_{x\zeta}^{(N_l)}(x,y,h/2) \quad \tau_{y\zeta}^{(N_l)}(x,y,h/2) \quad \sigma_\zeta^{(N_l)}(x,y,h/2) \quad D_\zeta^{(N_l)}(x,y,h/2)\right] = \left[0 \quad 0 \quad \bar{q}_\zeta^+(x,y) \quad 0\right] \text{ on the top surface, (24a)}$$

$$\left[\tau_{x\zeta}^{(1)}(x,y,-h/2) \quad \tau_{y\zeta}^{(1)}(x,y,-h/2) \quad \sigma_\zeta^{(1)}(x,y,-h/2) \quad D_\zeta^{(1)}(x,y,-h/2)\right] = \left[0 \quad 0 \quad 0 \quad 0\right], \text{ on the bottom surface; (24b)}$$

Case 4. Open-circuit surface conditions on which the electric normal displacements are applied,

$$\left[\tau_{x\zeta}^{(N_l)}(x,y,h/2) \quad \tau_{y\zeta}^{(N_l)}(x,y,h/2) \quad \sigma_\zeta^{(N_l)}(x,y,h/2) \quad D_\zeta^{(N_l)}(x,y,h/2)\right] = \left[0 \quad 0 \quad 0 \quad \bar{D}_\zeta^+(x,y)\right] \text{ on the top surface, (25a)}$$

$$\left[\tau_{x\zeta}^{(1)}(x,y,-h/2) \quad \tau_{y\zeta}^{(1)}(x,y,-h/2) \quad \sigma_\zeta^{(1)}(x,y,-h/2) \quad D_\zeta^{(1)}(x,y,-h/2)\right] = \left[0 \quad 0 \quad 0 \quad 0\right], \text{ on the bottom surface; (25b)}$$

where $\bar{q}_\zeta^+$, $\bar{\Phi}^+$ and $\bar{D}_\zeta^+$ are expressed as the double Fourier series and given as

$$\bar{q}_\zeta^+ = \sum_{\hat{m}=1}^{\infty} \sum_{\hat{n}=1}^{\infty} q_{\hat{m}\hat{n}} \sin(\tilde{m}\,x)\,\sin(\tilde{n}\,y), \quad \bar{\Phi}^+ = \sum_{\hat{m}=1}^{\infty} \sum_{\hat{n}=1}^{\infty} \phi_{\hat{m}\hat{n}} \sin(\tilde{m}\,x)\,\sin(\tilde{n}\,y) \quad \text{and} \quad \bar{D}_\zeta^+ = \sum_{\hat{m}=1}^{\infty} \sum_{\hat{n}=1}^{\infty} D_{3\hat{m}\hat{n}} \sin(\tilde{m}\,x)\,\sin(\tilde{n}\,y),$$

respectively, in which $\tilde{m} = \hat{m}\pi/L_x$, $\tilde{n} = \hat{n}\pi/L_y$ and $\hat{m}$, $\hat{n}$ are positive integers.

The edge boundary conditions of each individual layer are considered as fully simple supports with free electric potentials, which requires that the following quantities are satisfied.

$$u_y^{(m)} = u_\zeta^{(m)} = \sigma_x^{(m)} = \Phi^{(m)} = 0 \qquad \text{at } x=0, \ x=L_x \text{ and } m=1,2,\cdots,N_l \qquad (26a)$$

$$u_x^{(m)} = u_\zeta^{(m)} = \sigma_y^{(m)} = \Phi^{(m)} = 0, \qquad \text{at } y=0, \ y=L_y \text{ and } m=1,2,\cdots,N_l \qquad (26b)$$

By means of the separation of variables, the primary field variables of each individual layer are expanded as the following forms of a double Fourier series so that the boundary conditions of the simply supported edges are exactly satisfied. They are given as

$$\left(u_x^{(m)}, \ \tau_{x\zeta}^{(m)}\right) = \sum_{\hat{m}=1}^{\infty} \sum_{\hat{n}=1}^{\infty} \left(u_{\hat{m}\hat{n}}^{(m)}, \ \tau_{13\hat{m}\hat{n}}^{(m)}\right) \cos\tilde{m}\,x \ \sin\tilde{n}\,y \qquad (27)$$

$$\left(u_y^{(m)}, \ \tau_{y\zeta}^{(m)}\right) = \sum_{\hat{m}=1}^{\infty} \sum_{\hat{n}=1}^{\infty} \left(v_{\hat{m}\hat{n}}^{(m)}, \ \tau_{23\hat{m}\hat{n}}^{(m)}\right) \sin\tilde{m}\,x \ \cos\tilde{n}\,y \qquad (28)$$

$$\left(u_\zeta^{(m)}, \ \sigma_\zeta^{(m)}, \ D_\zeta^{(m)}, \ \Phi^{(m)}\right) = \sum_{\hat{m}=1}^{\infty} \sum_{\hat{n}=1}^{\infty} \left(w_{\hat{m}\hat{n}}^{(m)}, \ \sigma_{3\hat{m}\hat{n}}^{(m)}, \ D_{3\hat{m}\hat{n}}^{(m)}, \ \phi_{\hat{m}\hat{n}}^{(m)}\right) \sin\tilde{m}\,x \ \sin\tilde{n}\,y \qquad (29)$$

Introducing Eqs. (27)-(29) in Eq. (21) and imposing the stationary principle of the Reissner energy functional (i.e., $\delta\Pi_R = 0$), we obtain the Euler−Lagrange equations of the plate as follows

$$\sum_{m=1}^{N_l} \begin{bmatrix} \mathbf{K}_{\text{I I}}^{(m)} & \mathbf{0} & \mathbf{K}_{\text{I III}}^{(m)} & \mathbf{K}_{\text{I IV}}^{(m)} & \mathbf{K}_{\text{I V}}^{(m)} & \mathbf{0} \\ \mathbf{0} & \mathbf{0} & \mathbf{K}_{\text{II III}}^{(m)} & \mathbf{K}_{\text{II IV}}^{(m)} & \mathbf{0} & \mathbf{0} \\ \mathbf{K}_{\text{III I}}^{(m)} & \mathbf{K}_{\text{III II}}^{(m)} & \mathbf{K}_{\text{III III}}^{(m)} & \mathbf{0} & \mathbf{0} & \mathbf{K}_{\text{III VI}}^{(m)} \\ \mathbf{K}_{\text{IV I}}^{(m)} & \mathbf{K}_{\text{IV II}}^{(m)} & \mathbf{0} & \mathbf{K}_{\text{IV IV}}^{(m)} & \mathbf{K}_{\text{IV V}}^{(m)} & \mathbf{0} \\ \mathbf{K}_{\text{V I}}^{(m)} & \mathbf{0} & \mathbf{0} & \mathbf{K}_{\text{V IV}}^{(m)} & \mathbf{K}_{\text{V V}}^{(m)} & \mathbf{K}_{\text{V VI}}^{(m)} \\ \mathbf{0} & \mathbf{0} & \mathbf{K}_{\text{VI III}}^{(m)} & \mathbf{0} & \mathbf{K}_{\text{VI V}}^{(m)} & \mathbf{K}_{\text{VI VI}}^{(m)} \end{bmatrix} \begin{bmatrix} \tilde{\mathbf{u}}^{(m)} \\ \tilde{\mathbf{w}}^{(m)} \\ \tilde{\boldsymbol{\tau}}^{(m)} \\ \tilde{\boldsymbol{\sigma}}^{(m)} \\ \tilde{\mathbf{D}}^{(m)} \\ \tilde{\boldsymbol{\Phi}}^{(m)} \end{bmatrix} = \delta_{mN_l} \begin{bmatrix} \mathbf{0} \\ \mathbf{P}_\sigma \\ \mathbf{0} \\ \mathbf{0} \\ \mathbf{0} \\ \mathbf{P}_d \end{bmatrix} \qquad (30)$$

where $\mathbf{K}_{ij}^{(m)} = \left(\mathbf{K}_{ji}^{(m)}\right)^T$ $(i,j = \text{I, II, III, IV, V, VI})$; $\mathbf{K}_{\text{I I}}^{(m)} = \int_{-h_m/2}^{h_m/2} \left(\tilde{\mathbf{B}}_1^{(m)}\right)^T \mathbf{Q}_p^{(m)} \tilde{\mathbf{B}}_1^{(m)} \, dz_m$,

$\mathbf{K}_{\text{I III}}^{(m)} = \int_{-h_m/2}^{h_m/2} \left(\mathbf{B}_3^{(m)}\right)^T \mathbf{B}_5^{(m)} \, dz_m$, $\quad \mathbf{K}_{\text{I IV}}^{(m)} = \int_{-h_m/2}^{h_m/2} \left(\tilde{\mathbf{B}}_1^{(m)}\right)^T \mathbf{Q}_a^{(m)} \mathbf{B}_2^{(m)} \, dz_m$, $\quad \mathbf{K}_{\text{I V}}^{(m)} = \int_{-h_m/2}^{h_m/2} \left(\tilde{\mathbf{B}}_1^{(m)}\right)^T \mathbf{Q}_b^{(m)} \mathbf{B}_9^{(m)} \, dz_m$,

$\mathbf{K}_{\text{II III}}^{(m)} = \int_{-h_m/2}^{h_m/2} \left(\tilde{\mathbf{B}}_4^{(m)}\right)^T \mathbf{B}_5^{(m)} \, dz_m$, $\quad \mathbf{K}_{\text{II IV}}^{(m)} = \int_{-h_m/2}^{h_m/2} \left(\mathbf{B}_6^{(m)}\right)^T \mathbf{B}_2^{(m)} \, dz_m$, $\quad \mathbf{K}_{\text{III III}}^{(m)} = \int_{-h_m/2}^{h_m/2} \left(\mathbf{B}_5^{(m)}\right)^T \mathbf{S}_\sigma^{(m)} \mathbf{B}_5^{(m)} \, dz_m$,

$\mathbf{K}_{\text{III VI}}^{(m)} = \int_{-h_m/2}^{h_m/2} \left(\mathbf{B}_5^{(m)}\right)^T \mathbf{S}_e^{(m)} \tilde{\mathbf{B}}_7^{(m)} \, dz_m$, $\quad \mathbf{K}_{\text{IV IV}}^{(m)} = -\int_{-h_m/2}^{h_m/2} \bar{\eta}^{(m)} \left(\mathbf{B}_2^{(m)}\right)^T \mathbf{B}_2^{(m)} \, dz_m$,

$$\mathbf{K}_{\mathrm{IV\,V}}^{(m)} = -\int_{-h_m/2}^{h_m/2} \bar{e}^{(m)} \left(\mathbf{B}_2^{(m)}\right)^T \mathbf{B}_9^{(m)} \, dz_m \;, \quad \mathbf{K}_{\mathrm{V\,V}}^{(m)} = \int_{-h_m/2}^{h_m/2} \bar{c}^{(m)} \left(\mathbf{B}_9^{(m)}\right)^T \mathbf{B}_9^{(m)} \, dz_m \;,$$

$$\mathbf{K}_{\mathrm{V\,VI}}^{(m)} = \int_{-h_m/2}^{h_m/2} \left(\mathbf{B}_9^{(m)}\right)^T \mathbf{B}_8^{(m)} \, dz_m \;, \quad \mathbf{K}_{\mathrm{VI\,VI}}^{(m)} = -\int_{-h_m/2}^{h_m/2} \left(\widetilde{\mathbf{B}}_7^{(m)}\right)^T \mathbf{S}_\eta^{(m)} \widetilde{\mathbf{B}}_7^{(m)} \, dz_m \;,$$

$$\widetilde{\mathbf{B}}_1^{(m)} = \begin{bmatrix} -\tilde{m}\left(\psi_u^{(m)}\right)_i & 0 \\ 0 & -\tilde{n}\left(\psi_u^{(m)}\right)_i \\ \tilde{n}\left(\psi_u^{(m)}\right)_i & \tilde{m}\left(\psi_u^{(m)}\right)_i \end{bmatrix}_{i=1,2,\cdots,n_u+1} \;, \quad \widetilde{\mathbf{B}}_4^{(m)} = \begin{bmatrix} \tilde{m}\left(\psi_w^{(m)}\right)_i \\ \tilde{n}\left(\psi_w^{(m)}\right)_i \end{bmatrix}_{i=1,2,\cdots,n_w+1} \;, \quad \widetilde{\mathbf{B}}_7^{(m)} = \begin{bmatrix} \tilde{m}\left(\psi_\phi^{(m)}\right)_i \\ \tilde{n}\left(\psi_\phi^{(m)}\right)_i \end{bmatrix}_{i=1,2,\cdots,n_\phi+1} \;,$$

$$\widetilde{\mathbf{u}}^{(m)} = \begin{bmatrix} \left(u_{\hat{m}\hat{n}}^{(m)}\right)_i \\ \left(v_{\hat{m}\hat{n}}^{(m)}\right)_i \end{bmatrix}_{i=1,2,\cdots,n_u+1} \;, \quad \widetilde{\mathbf{w}}^{(m)} = \left[\left(w_{\hat{m}\hat{n}}^{(m)}\right)_i\right]_{i=1,2,\cdots,n_w+1} \;, \quad \widetilde{\boldsymbol{\tau}}^{(m)} = \begin{bmatrix} \left(\tau_{13\hat{m}\hat{n}}^{(m)}\right)_i \\ \left(\tau_{23\hat{m}\hat{n}}^{(m)}\right)_i \end{bmatrix}_{i=1,2,\cdots,n_\tau+1}$$

$$\widetilde{\boldsymbol{\sigma}}^{(m)} = \left[\left(\sigma_{3\hat{m}\hat{n}}^{(m)}\right)_i\right]_{i=1,2,\cdots,n_\sigma+1} \;, \quad \widetilde{D}^{(m)} = \left[\left(D_{3\hat{m}\hat{n}}^{(m)}\right)_i\right]_{i=1,2,\cdots,n_d+1} \;, \quad \widetilde{\Phi}^{(m)} = \left[\left(\phi_{\hat{m}\hat{n}}^{(m)}\right)_i\right]_{i=1,2,\cdots,n_\phi+1} \;,$$

$$\mathbf{P}_\sigma = \left(q_{\hat{m}\hat{n}}\right)\left[\delta_{i(n_w+1)}\right]_{i=1,2,\cdots,n_w+1} \;, \quad \mathbf{P}_d = \left(D_{3\hat{m}\hat{n}}\right)\left[\delta_{i(n_d+1)}\right]_{i=1,2,\cdots,n_d+1} \;;$$

and the symbols of δ_{mN_l} $\left(m=1,2,\cdots,N_l\right)$ and $\delta_{i(n_k+1)}$ $\left(i=1,2,\cdots,n_k+1\right)$ are the Kronecker delta functions, in which $k=u,\ w,\ d$ and ϕ.

Using Eq. (30) and assembling the local stiffness matrix and forcing vector of each layer, in which the elastic displacement, transverse stress, electric potential and normal electric displacement continuity conditions at the interfaces between adjacent layers are imposed, and thus satisfied a priori for the RMVT-based FLMs, we may construct the global stiffness matrix and forcing vector for the plate. The primary variables at each nodal plane can then be determined. Subsequently, the variables of in-plane stress and electric displacement components at the nodal planes can be obtained using the determined primary variables, and these are given by

$$\left(\sigma_x^{(m)},\ \sigma_y^{(m)}\right) = \sum_{\hat{m}=1}^{\infty}\sum_{\hat{n}=1}^{\infty} \left(\sigma_{1\hat{m}\hat{n}}^{(m)},\ \sigma_{2\hat{m}\hat{n}}^{(m)}\right) \sin\tilde{m}x \ \sin\tilde{n}y \tag{31}$$

$$\tau_{xy}^{(m)} = \sum_{\hat{m}=1}^{\infty}\sum_{\hat{n}=1}^{\infty} \tau_{12\hat{m}\hat{n}}^{(m)} \ \cos\tilde{m}x \ \cos\tilde{n}y \tag{32}$$

$$D_x^{(m)} = \sum_{\hat{m}=1}^{\infty}\sum_{\hat{n}=1}^{\infty} D_{1\hat{m}\hat{n}}^{(m)} \ \cos\tilde{m}x \ \sin\tilde{n}y \tag{33}$$

$$D_y^{(m)} = \sum_{\hat{m}=1}^{\infty}\sum_{\hat{n}=1}^{\infty} D_{2\hat{m}\hat{n}}^{(m)} \ \sin\tilde{m}x \ \cos\tilde{n}y \tag{34}$$

where $\begin{bmatrix} \sigma_{1\hat{m}\hat{n}}^{(m)} & \sigma_{2\hat{m}\hat{n}}^{(m)} & \tau_{12\hat{m}\hat{n}}^{(m)} \end{bmatrix}^T = \mathbf{Q}_p^{(m)} \widetilde{\mathbf{B}}_1^{(m)} \widetilde{\mathbf{u}}^{(m)} + \mathbf{Q}_a^{(m)} \mathbf{B}_2^{(m)} \widetilde{\boldsymbol{\sigma}}^{(m)} + \mathbf{Q}_b^{(m)} \mathbf{B}_9^{(m)} \widetilde{\mathbf{D}}^{(m)}$,

and $\begin{bmatrix} D_{1\hat{m}\hat{n}}^{(m)} & D_{2\hat{m}\hat{n}}^{(m)} \end{bmatrix}^T = \mathbf{S}_e^{(m)} \mathbf{B}_5^{(m)} \widetilde{\boldsymbol{\tau}}^{(m)} - \mathbf{S}_\eta^{(m)} \widetilde{\mathbf{B}}_7^{(m)} \widetilde{\boldsymbol{\Phi}}^{(m)}$.
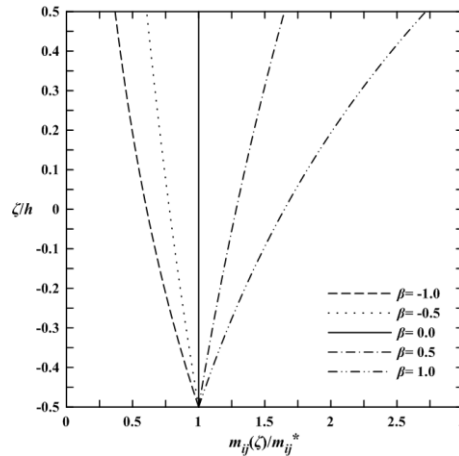
Fig. 2 The through-thickness distributions of the material properties of a single-layered FGPM plate, in which β =-1.0, -0.5, 0.0, 0.5, 1.0

Using this unified formulation of RMVT-based FLMs, we may analyze the 3D coupled electro-elastic behaviors of single- and multi-layered FGPM plates and laminated homogeneous piezoelectric ones with closed- and open-circuit surface conditions and under electro-mechanical loads, and the performances of various RMVT-based FLMs with different orders used for expanding the electric and elastic field variables in the thickness coordinate will be also examined later in this article.

3. Illustrative examples

The unified formulation of RMVT- based FLMs for the FGPM plates was presented above, in which various combinations of the orders used for expanding the elastic displacement, electric potential, transverse stress and normal electric displacement components in the thickness coordinate can be freely chosen. The acronyms, $LM_{n_u\ n_w\ n_\phi}^{n_\tau\ n_\sigma\ n_d}$, are thus defined to represent various RMVT-based FLMs, in which the in- and out-of-plane elastic displacements and the electric potential are expanded as the n_u-, n_w- and n_ϕ-order Lagrange polynomials, respectively, and the transverse shear and normal stresses and the normal electric displacement are expanded as the n_τ-, n_σ- and n_d-order Lagrange polynomials in the thickness coordinate of each layer, respectively. The values of n_i ($i = u$, w, τ and σ) remain the same, and are taken to be less than 4, namely 1(linear), 2(quadratic) and 3(cubic) in the following examples.

3.1 Single-layered FGPM plates

In this section, the static behavior of a simply-supported, single-layered FGPM plate with the loading cases 1 and 2 is investigated, which has been also examined by Lu *et al*. (2006) using the PSF and Brischetto and Carrera (2009) using CUF, and their solutions are used to evaluate the accuracy and convergence rate of the FLMs with different orders. PZT-4 is used as the reference

material, the material properties of which are given in Table 1, and this is placed in the bottom of the plate. The material properties of the plate are assumed to vary exponentially through the thickness coordinate, and are given by

Table 1 Elastic, piezoelectric and dielectric coefficients of composite and piezoelectric materials

Moduli	PZT-4 (Lu *et al.* 2006)
c_{11} (GPa)	139
c_{22} (GPa)	139
c_{33} (GPa)	115
c_{12} (GPa)	77.8
c_{13} (GPa)	74.3
c_{23} (GPa)	74.3
c_{44} (Gpa)	25.6
c_{55} (Gpa)	25.6
c_{66} (Gpa)	30.6
e_{24} (C/m^2)	12.7
e_{15} (C/m^2)	12.7
e_{31} (C/m^2)	-5.2
e_{32} (C/m^2)	-5.2
e_{33} (C/m^2)	15.1
η_{11}/η_0 (F/m)	1475
η_{22}/η_0 (F/m)	1475
η_{33}/η_0 (F/m)	1300

η_0 denotes the dielectric permittivity of free space, and $\eta_0 = 8.854e\text{-}12$ (F/m)

Table 2 Results of convergence rate and accuracy studies for the FLM solutions of electric and elastic variables induced at the position $x=y=0.25L_x$ in a single-layered FGPM plate under mechanical loads (Case 1) ($L_x = L_y = 1\text{m}$, $L_x/h = 10$)

β	Theories	$10^{11}\,u_x$ ($\zeta = 0$)	$10^9\,u_\zeta$ ($\zeta = 0$)	σ_x ($\zeta = -h/2$)	τ_{xy} ($\zeta = h/2$)	σ_ζ ($\zeta = h/2$)	$10^2\,\Phi$ ($\zeta = 0$)	$10^9\,D_\zeta$ ($\zeta = 0$)
-1.0	$\text{LM}_{111}^{111}(N_l = 4)$	0.674	-0.253	15.403	3.101	-0.485	-0.600	0.328
	$\text{LM}_{111}^{111}(N_l = 8)$	0.673	-0.253	15.40	3.103	-0.497	-0.602	0.332
	$\text{LM}_{111}^{111}(N_l = 12)$	0.673	-0.253	15.40	3.103	-0.499	-0.602	0.332
	$\text{LM}_{111}^{111}(N_l = 16)$	0.673	-0.253	15.40	3.103	-0.499	-0.602	0.332
	$\text{LM}_{222}^{222}(N_l = 4)$	0.674	-0.253	15.40	3.103	-0.495	-0.602	0.332
	$\text{LM}_{222}^{222}(N_l = 8)$	0.673	-0.253	15.40	3.103	-0.499	-0.602	0.332
	$\text{LM}_{222}^{222}(N_l = 12)$	0.673	-0.253	15.40	3.103	-0.500	-0.602	0.333
	$\text{LM}_{222}^{222}(N_l = 16)$	0.673	-0.253	15.40	3.103	-0.500	-0.602	0.333
	$\text{LM}_{333}^{333}(N_l = 4)$	0.673	-0.253	15.40	3.103	-0.500	-0.602	0.333
	$\text{LM}_{333}^{333}(N_l = 8)$	0.673	-0.253	15.40	3.103	-0.500	-0.602	0.333
	$\text{LM}_{333}^{333}(N_l = 12)$	0.673	-0.253	15.40	3.103	-0.500	-0.602	0.333
	$\text{LM}_{333}^{333}(N_l = 16)$	0.673	-0.253	15.40	3.103	-0.500	-0.602	0.333
	3D (Lu et al., 2006)	0.650	-0.251	15.23	3.041	-0.500	-0.596	0.312
	CUF (Brischetto and Carrera, 2009)	0.647	-0.248	15.21	3.039	-0.511	-0.591	0.316
0.0	$\text{LM}_{111}^{111}(N_l = 4)$	-0.029	-0.151	10.95	4.244	-0.506	-0.392	-0.059
	$\text{LM}_{111}^{111}(N_l = 8)$	-0.029	-0.151	10.96	4.246	-0.502	-0.393	-0.059
	$\text{LM}_{111}^{111}(N_l = 12)$	-0.029	-0.151	10.96	4.246	-0.501	-0.393	-0.059
	$\text{LM}_{111}^{111}(N_l = 16)$	-0.029	-0.151	10.96	4.246	-0.500	-0.393	-0.059
	$\text{LM}_{222}^{222}(N_l = 4)$	-0.029	-0.151	10.96	4.246	-0.501	-0.393	-0.059
	$\text{LM}_{222}^{222}(N_l = 8)$	-0.029	-0.151	10.96	4.246	-0.500	-0.393	-0.059
	$\text{LM}_{222}^{222}(N_l = 12)$	-0.029	-0.151	10.96	4.246	-0.500	-0.393	-0.059
	$\text{LM}_{222}^{222}(N_l = 16)$	-0.029	-0.151	10.96	4.246	-0.500	-0.394	-0.059
	$\text{LM}_{333}^{333}(N_l = 4)$	-0.029	-0.151	10.96	4.246	-0.500	-0.394	-0.059
	$\text{LM}_{333}^{333}(N_l = 8)$	-0.029	-0.151	10.96	4.246	-0.500	-0.394	-0.059
	$\text{LM}_{333}^{333}(N_l = 12)$	-0.029	-0.151	10.96	4.246	-0.500	-0.394	-0.059
	$\text{LM}_{333}^{333}(N_l = 16)$	-0.029	-0.151	10.96	4.246	-0.500	-0.394	-0.059
	3D (Lu *et al.* 2006)	-0.031	-0.151	10.92	4.247	-0.500	-0.393	-0.061
	CUF (Brischetto and Carrera 2009)	-0.029	-0.151	10.96	4.241	-0.500	-0.393	-0.059
1.0	$\text{LM}_{111}^{111}(N_l = 4)$	-0.284	-0.094	7.623	5.844	-0.521	-0.221	-0.445
	$\text{LM}_{111}^{111}(N_l = 8)$	-0.284	-0.094	7.629	5.847	-0.505	-0.221	-0.449
	$\text{LM}_{111}^{111}(N_l = 12)$	-0.284	-0.094	7.629	5.847	-0.502	-0.221	-0.450
	$\text{LM}_{111}^{111}(N_l = 16)$	-0.284	-0.094	7.629	5.847	-0.501	-0.221	-0.451
	$\text{LM}_{222}^{222}(N_l = 4)$	-0.284	-0.094	7.629	5.847	-0.504	-0.221	-0.450
	$\text{LM}_{222}^{222}(N_l = 8)$	-0.284	-0.094	7.629	5.847	-0.501	-0.221	-0.451
	$\text{LM}_{222}^{222}(N_l = 12)$	-0.284	-0.094	7.629	5.847	-0.500	-0.221	-0.451

Continued-

$\mathrm{LM}_{222}^{222}(N_l = 16)$	-0.284	-0.094	7.629	5.847	-0.500	-0.221	-0.451
$\mathrm{LM}_{333}^{333}(N_l = 4)$	-0.284	-0.094	7.629	5.847	-0.500	-0.221	-0.451
$\mathrm{LM}_{333}^{333}(N_l = 8)$	-0.284	-0.094	7.629	5.847	-0.500	-0.221	-0.451
$\mathrm{LM}_{333}^{333}(N_l = 12)$	-0.284	-0.094	7.629	5.847	-0.500	-0.221	-0.451
$\mathrm{LM}_{333}^{333}(N_l = 16)$	-0.284	-0.094	7.629	5.847	-0.500	-0.221	-0.451
3D (Lu *et al.* 2006)	-0.275	-0.094	7.529	5.830	-0.500	-0.220	-0.445
CUF (Brischetto and Carrera 2009)	-0.273	-0.092	7.504	5.773	-0.481	-0.217	-0.432

$$m_{ij}(\zeta) = m_{ij}^{*} \, e^{\beta[(\zeta/h)+(1/2)]} \tag{35}$$

in which m_{ij}^{*} denotes the material properties of PZT-4, β is the material-property gradient index, and $(-h/2) \leq \zeta \leq (h/2)$. The through-thickness distributions of material properties are shown in Fig. 2, in which $\beta = -1.0, -0.5, 0, 0.5$ and 1.0.

Tables 2 and 3 show the LM_{111}^{111}, LM_{222}^{222} and LM_{333}^{333} solutions of various electric and elastic variables induced at some specific positions $(L_x/4, L_y/4, \zeta)$ of the plates subjected to the sinusoidally distributed mechanical load and electric potential (i.e., $\overline{q}_{\zeta}^{+} = q_0 \sin(\pi x/L_x)\sin(\pi y/L_y)$, $\overline{q}_{\zeta}^{-} = 0$, and $\overline{\Phi}^{+} = \phi_0 \sin(\pi x/L_x)\sin(\pi y/L_y)$, $\overline{\Phi}^{-} = 0$), respectively, in which $L_x = L_y = 1\,\mathrm{m}$, $S = L_x/h = 10$ and $N_l = 4, 8, 12, 16$ and 32. It can be seen in Tables 2 and 3 that the accuracy based on the same value of N_l and convergence rate for various FLMs are $\mathrm{LM}_{333}^{333} > \mathrm{LM}_{222}^{222} > \mathrm{LM}_{111}^{111}$, in which the symbol ">" means more accurate and more rapid, which is more obvious for the transverse normal stress and normal electric displacement components than for the others. It is also shown that the 32-layer LM_{111}^{111}, 12-layer LM_{222}^{222}, and 4-layer LM_{333}^{333} solutions are in excellent agreement with the exact 3D solutions and CUF ones available in the literature, in which the relative errors of various FLM solutions of all electric and elastic variables will be lower than 1% as compared with the 3D solutions. The RMVT-based FLMs with cubic orders are thus used in the later work in this article.

3.2 Two-layered FGPM film/substrate plates

In this section, we consider a simply-supported, two-layered FGPM film-substrate plates (FSP) under electro-mechanical loads. The substrate is a homogenous PZT-4 layer with a thickness h_1, and the film is an FGPM one with a thickness h_2 bounded on the top surface of the substrate, while $h_1 + h_2 = h$. The material properties of the FSP through the thickness coordinate are expressed as follows

$$m_{ij}(\zeta) = m_{ij}^{*} \qquad\qquad (-h/2) \leq \zeta \leq -(h/2 - h_1) \tag{36a}$$

$$m_{ij}(\zeta) = m_{ij}^{*} \, e^{\beta\{[\zeta-(-h/2+h_1)]/h_2\}} \qquad -(h/2 - h_1) \leq \zeta \leq (h/2) \tag{36b}$$

in which the material properties are continuous at the film-substrate interface, and the through-thickness distributions of these are shown in Fig. 3 in the case of $h_1 = h_2 = h/2$ and $\beta = -1.0, -0.5, 0.0, 0.5$ and 1.0.

The loading conditions of Cases 1 and 3 are $\bar{q}_\zeta^+ = q_0 \sin(\pi x / L_x)\sin(\pi y / L_y)$, $\bar{q}_\zeta^- = 0$, and those of Cases 2 and 4 are $\bar{\Phi}^+ = \phi_0 \sin(\pi x / L_x)\sin(\pi y / L_y)$, $\bar{\Phi}^- = 0$, and $\bar{D}_\zeta^+ = D_0 \sin(\pi x / L_x)\sin(\pi y / L_y)$, $\bar{D}_\zeta^- = 0$, respectively. The sets of dimensionless field variables for the different loading cases 1-4 are defined as follows:

For the cases of applied mechanical loads (Cases 1 and 3),

$$[\bar{u}_x, \quad \bar{u}_\zeta] = [u_x, \quad u_\zeta] c_{33}^* / (q_0 S^4 h), \quad [\bar{\sigma}_x, \quad \bar{\tau}_{x\zeta}, \quad \bar{\sigma}_\zeta] = [\sigma_x / (S^2 q_0), \quad \tau_{x\zeta} / (S q_0), \quad \sigma_\zeta / q_0],$$

$$[\bar{\Phi}, \quad \bar{D}_\zeta] = [\Phi e_{33}^* / (q_0 S^2 h), \quad D_\zeta c_{33}^* / (q_0 S e_{33}^*)], \quad S = L_x / h \tag{37a-d}$$

For the cases of applied electric potential (Case 2),

$$[\bar{u}_x, \quad \bar{u}_\zeta] = [u_x, \quad u_\zeta] c_{33}^* / (\phi_0 S e_{33}^*), \quad [\bar{\sigma}_x, \quad \bar{\tau}_{x\zeta}, \quad \bar{\sigma}_\zeta] = [Sh\sigma_x, \quad S^2 h\tau_{x\zeta}, \quad S^3 h\sigma_\zeta] / (\phi_0 e_{33}^*),$$

$$[\bar{\Phi}, \quad \bar{D}_\zeta] = [\Phi / \phi_0, \quad D_\zeta (c_{33}^* h) / (\phi_0 (e_{33}^*)^2)] \tag{38a-c}$$

Table 3 Results of convergence rate and accuracy studies for the FLM solutions of electric and elastic variables induced at the position $x=y=0.25L_x$ in a single-layered FGPM plate under electric potential (Case 2) ($L_x = L_y = 1\text{m}$, $L_x / h = 10$)

β	Theories	$10^9 u_x$ ($\zeta = 0$)	$10^9 u_\zeta$ ($\zeta = 0$)	σ_x ($\zeta = -h/2$)	τ_{xy} ($\zeta = h/2$)	σ_ζ ($\zeta = h/2$)	Φ ($\zeta = 0$)	$10^7 D_\zeta$ ($\zeta = 0$)
-1.0	$\mathbf{LM}_{111}^{111}(N_l = 4)$	-0.129	0.338	-16.50	-14.30	0.202	0.183	-0.448
	$\mathbf{LM}_{111}^{111}(N_l = 8)$	-0.129	0.338	-17.41	-14.30	0.050	0.183	-0.455
	$\mathbf{LM}_{111}^{111}(N_l = 12)$	-0.129	0.338	-17.58	-14.30	0.022	0.183	-0.456
	$\mathbf{LM}_{111}^{111}(N_l = 16)$	-0.129	0.338	-17.64	-14.30	0.013	0.183	-0.457
	$\mathbf{LM}_{111}^{111}(N_l = 32)$	-0.129	0.338	-17.70	-14.30	0.003	0.183	-0.457
	$\mathbf{LM}_{222}^{222}(N_l = 4)$	-0.129	0.338	-17.33	-14.30	0.053	0.183	-0.454
	$\mathbf{LM}_{222}^{222}(N_l = 8)$	-0.129	0.338	-17.62	-14.30	0.013	0.183	-0.457
	$\mathbf{LM}_{222}^{222}(N_l = 12)$	-0.129	0.338	-17.67	-14.30	0.006	0.183	-0.457
	$\mathbf{LM}_{222}^{222}(N_l = 16)$	-0.129	0.338	-17.69	-14.30	0.003	0.183	-0.457
	$\mathbf{LM}_{333}^{333}(N_l = 4)$	-0.129	0.338	-17.71	-14.30	-0.000	0.183	-0.457
	$\mathbf{LM}_{333}^{333}(N_l = 8)$	-0.129	0.338	-17.71	-14.30	-0.000	0.183	-0.457
	$\mathbf{LM}_{333}^{333}(N_l = 12)$	-0.129	0.338	-17.72	-14.30	-0.000	0.183	-0.457
	$\mathbf{LM}_{333}^{333}(N_l = 16)$	-0.129	0.338	-17.72	-14.30	-0.000	0.183	-0.457
	3D (Lu *et al.* 2006)	-0.129	0.327	-18.06	-14.22	0.000	0.181	-0.457
	CUF (Brischetto and Carrera 2009)	-0.125	0.325	-18.04	-13.80	0.002	0.183	-0.455
0.0	$\mathbf{LM}_{111}^{111}(N_l = 4)$	-0.129	-0.072	-23.17	-27.25	0.390	0.243	-0.785
	$\mathbf{LM}_{111}^{111}(N_l = 8)$	-0.129	-0.072	-23.63	-27.25	0.098	0.243	-0.788
	$\mathbf{LM}_{111}^{111}(N_l = 12)$	-0.129	-0.072	-23.71	-27.25	0.044	0.243	-0.789

Continued-

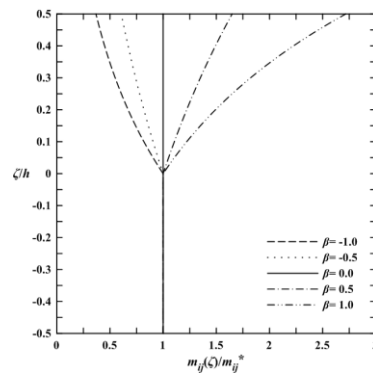|							
	$LM_{111}^{111}(N_l=16)$	-0.129	-0.072	-23.74	-27.25	0.025	0.243	-0.789
	$LM_{111}^{111}(N_l=32)$	-0.129	-0.072	-23.77	-27.25	0.006	0.243	-0.789
	$LM_{222}^{222}(N_l=4)$	-0.129	-0.072	-23.62	-27.25	0.099	0.243	-0.788
	$LM_{222}^{222}(N_l=8)$	-0.129	-0.072	-23.74	-27.25	0.025	0.243	-0.789
	$LM_{222}^{222}(N_l=12)$	-0.129	-0.072	-23.76	-27.25	0.011	0.243	-0.789
	$LM_{222}^{222}(N_l=16)$	-0.129	-0.072	-23.77	-27.25	0.006	0.243	-0.789
	$LM_{333}^{333}(N_l=4)$	-0.129	-0.072	-23.78	-27.25	0.000	0.243	-0.789
	$LM_{333}^{333}(N_l=8)$	-0.129	-0.072	-23.78	-27.25	0.000	0.243	-0.789
	$LM_{333}^{333}(N_l=12)$	-0.129	-0.072	-23.78	-27.25	0.000	0.243	-0.789
	$LM_{333}^{333}(N_l=16)$	-0.129	-0.072	-23.78	-27.25	0.000	0.243	-0.789
	3D (Lu *et al.* 2006)	-0.129	-0.074	-23.79	-27.19	0.000	0.242	-0.787
	CUF (Brischetto and Carrera 2009)	-0.128	-0.072	-23.68	-27.16	0.005	0.243	-0.788
1.0	$LM_{111}^{111}(N_l=4)$	-0.129	-0.487	-40.85	-41.95	0.616	0.302	-1.232
	$LM_{111}^{111}(N_l=8)$	-0.129	-0.487	-42.92	-41.95	0.154	0.303	-1.250
	$LM_{111}^{111}(N_l=12)$	-0.129	-0.487	-43.31	-41.95	0.068	0.303	-1.253
	$LM_{111}^{111}(N_l=16)$	-0.129	-0.487	-43.45	-41.95	0.038	0.303	-1.254
	$LM_{111}^{111}(N_l=32)$	-0.129	-0.487	-43.58	-41.95	0.010	0.303	-1.255
	$LM_{222}^{222}(N_l=4)$	-0.129	-0.487	-42.79	-41.95	0.155	0.303	-1.249
	$LM_{222}^{222}(N_l=8)$	-0.129	-0.487	-43.41	-41.95	0.039	0.303	-1.254
	$LM_{222}^{222}(N_l=12)$	-0.129	-0.487	-43.53	-41.95	0.017	0.303	-1.255
	$LM_{222}^{222}(N_l=16)$	-0.129	-0.487	-43.57	-41.95	0.010	0.303	-1.255
	$LM_{333}^{333}(N_l=4)$	-0.129	-0.487	-43.62	-41.95	-0.001	0.303	-1.256
	$LM_{333}^{333}(N_l=8)$	-0.129	-0.487	-43.62	-41.95	-0.000	0.303	-1.256
	$LM_{333}^{333}(N_l=12)$	-0.129	-0.487	-43.62	-41.95	-0.000	0.303	-1.256
	$LM_{333}^{333}(N_l=16)$	-0.129	-0.487	-43.62	-41.95	0.000	0.303	-1.256
	3D (Lu *et al.* 2006)	-0.129	-0.480	-44.27	-41.72	0.000	0.300	-1.257
	CUF (Brischetto and Carrera 2009)	-0.125	-0.466	-45.61	-41.00	0.001	0.303	-1.249

Fig. 3 The through-thickness distributions of the material properties of an FGPM FSP, in which $h_1 : h_2 = 0.5h : 0.5h$ and $\beta = -1.0, -0.5, 0.0, 0.5, 1.0$
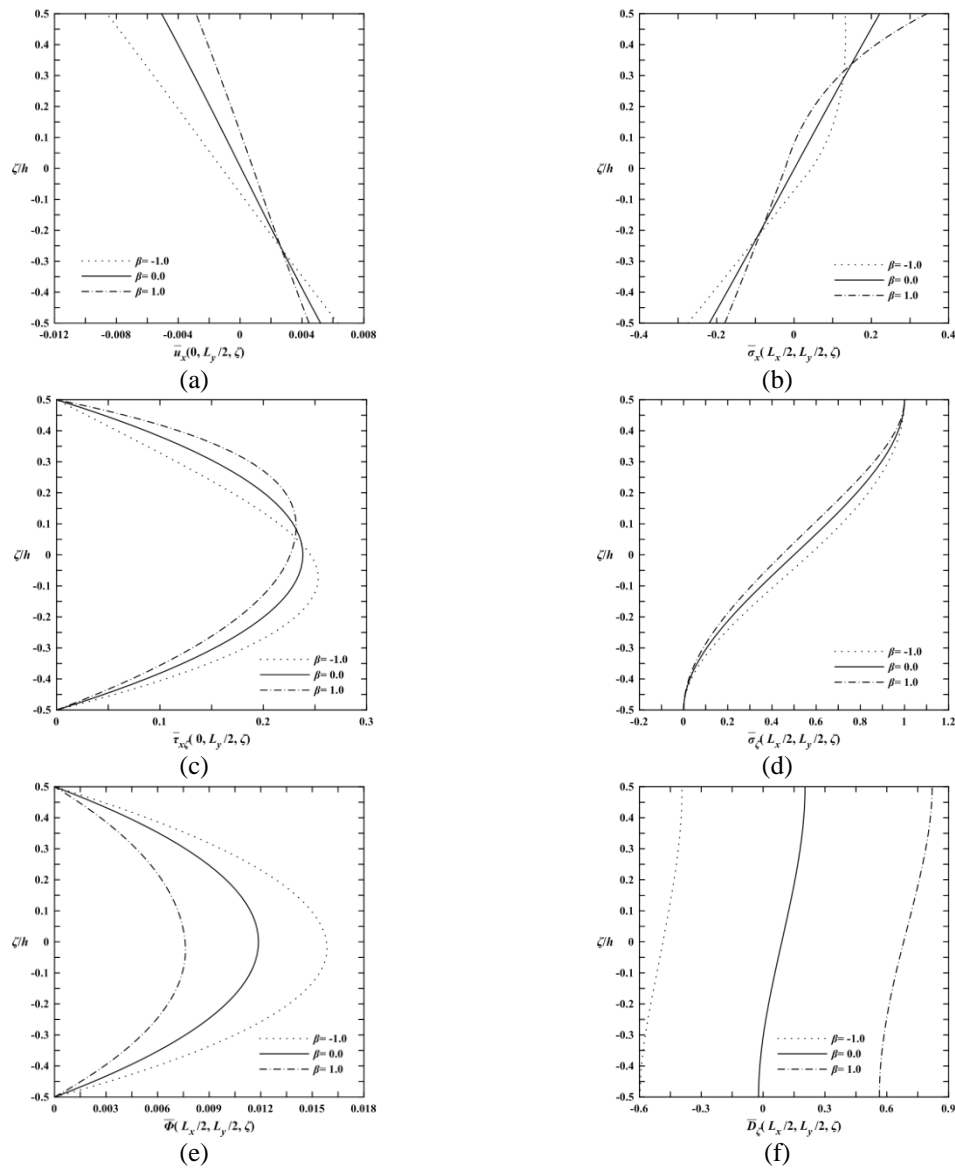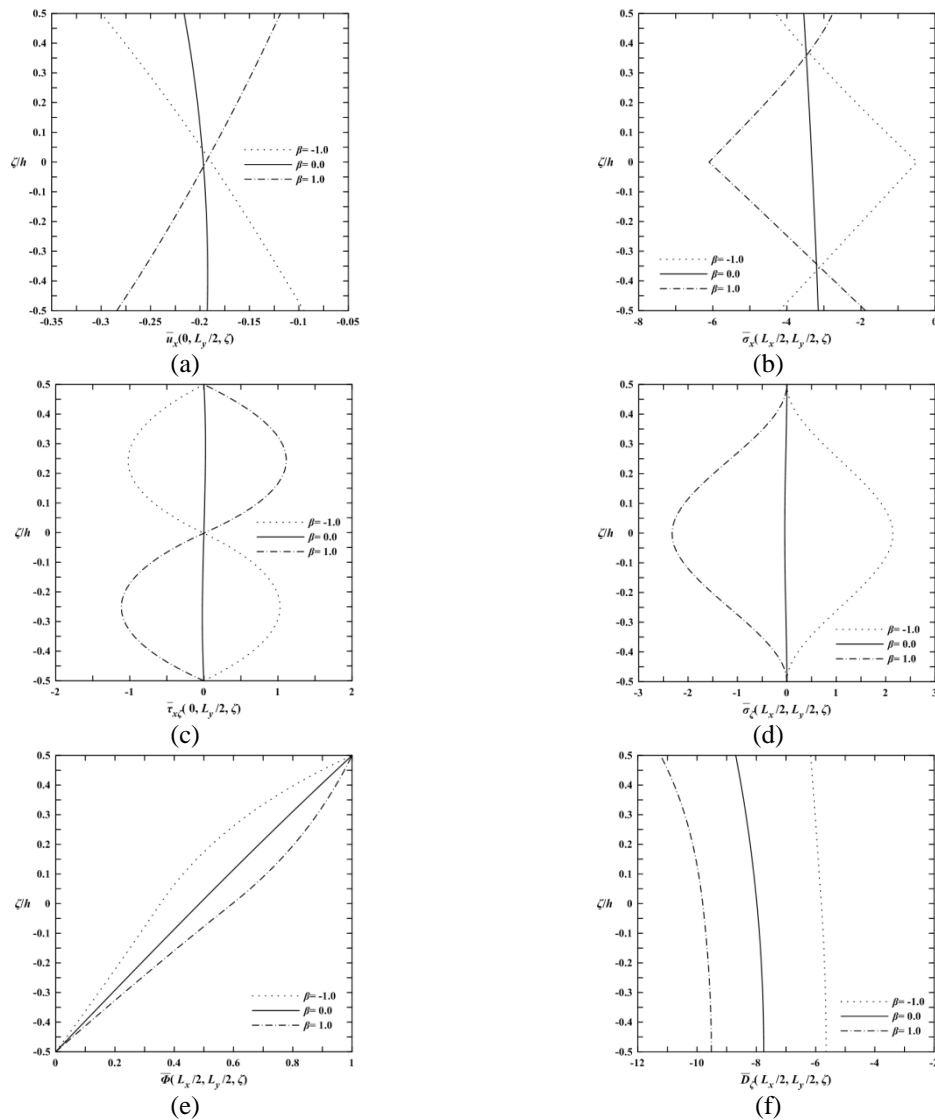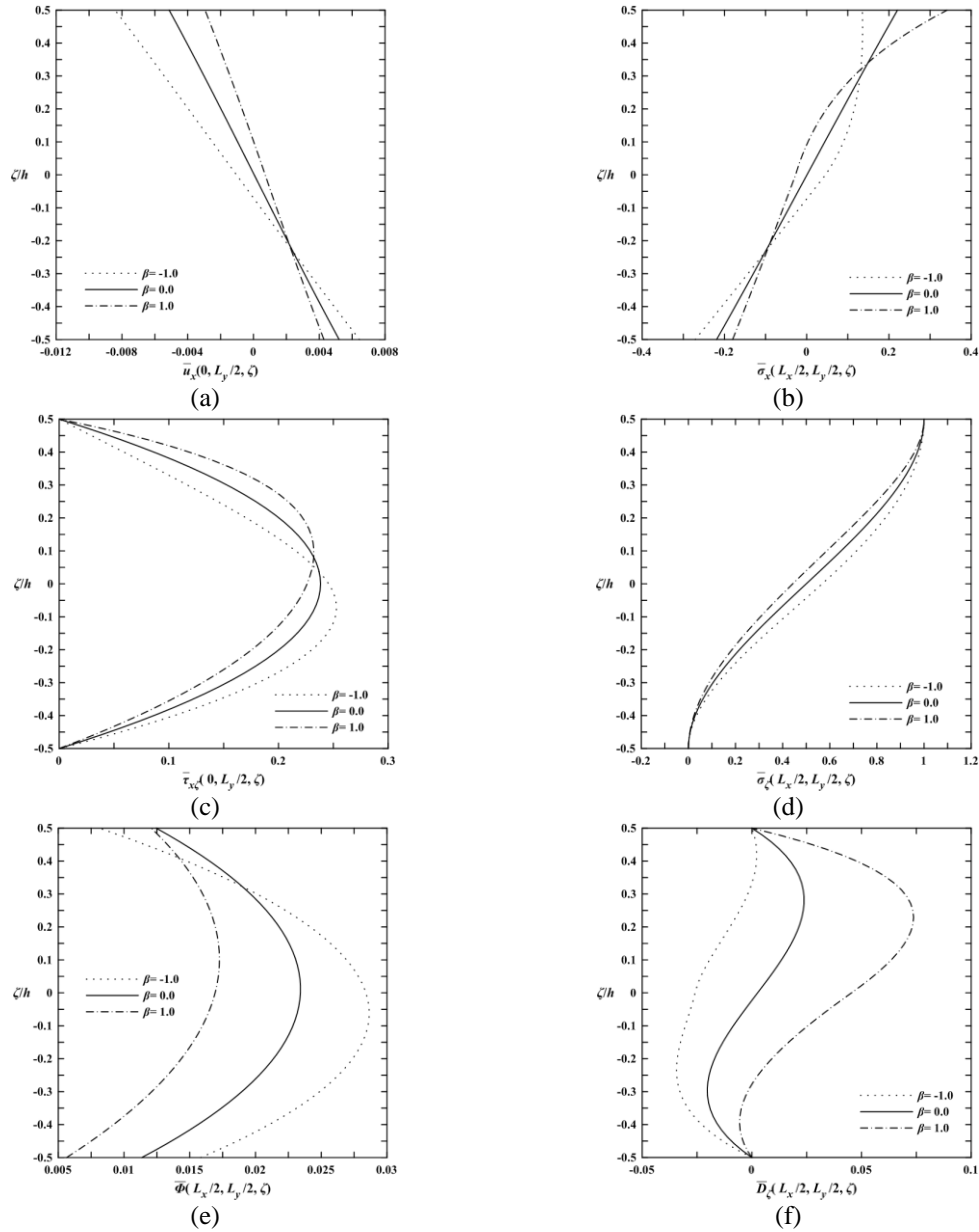
Fig. 4 The through-thickness distributions of various elastic and electric variables induced in an FGPM FSP for loading Case 1, in which β =-1.0, 0.0 and 1.0, $h_1 : h_2 = 0.5h : 0.5h$, and $L_x / h = 10$, $L_x = L_y$

For the cases of applied normal electric displacement (Case 4),

$$\left[\overline{u}_x, \quad \overline{u}_\zeta \right] = \left[u_x, \quad u_\zeta \right] e_{33}^* / (D_0 \, S \, h), \quad \left[\overline{\sigma}_x, \quad \overline{\tau}_{x\zeta}, \quad \overline{\sigma}_\zeta \right] = \left[S e_{33}^* \sigma_x, \quad S^2 e_{33}^* \tau_{x\zeta}, \quad S^3 e_{33}^* \sigma_\zeta \right] / (D_0 \, c_{33}^*) ,$$

$$\left[\overline{\Phi}, \quad \overline{D}_\zeta \right] = \left[\Phi \left(e_{33}^* \right)^2 / \left(D_0 \, c_{33}^* \, h \right), \quad D_\zeta / D_0 \right] \tag{39a-c}$$

in which c_{33}^* and e_{33}^* denote the corresponding material properties of PZT-4.

Figs. 4-7 show the through-thickness distributions of electric and elastic variables induced in the FGPM film-substrate plate for the loading conditions of Cases 1-4, respectively, in which L_x/h=10, L_x=L_y, β =-1.0, 0 and 1.0. When β =0, the FGPM FSP becomes a single-layered homogeneous PZT-4 plate. It can be seen in Figs. 4 and 6 that in the cases of applied mechanical loads (Cases 1 and 3), the in-plane elastic displacement and stress, transverse shear stress, and transverse normal stress variables appear to be the linear, parabolic and higher-order polynomial variations through the thickness coordinate for the homogeneous piezoelectric plates (β =0), while those for FGPM FSPs change more dramatically than those for homogeneous piezoelectric ones.
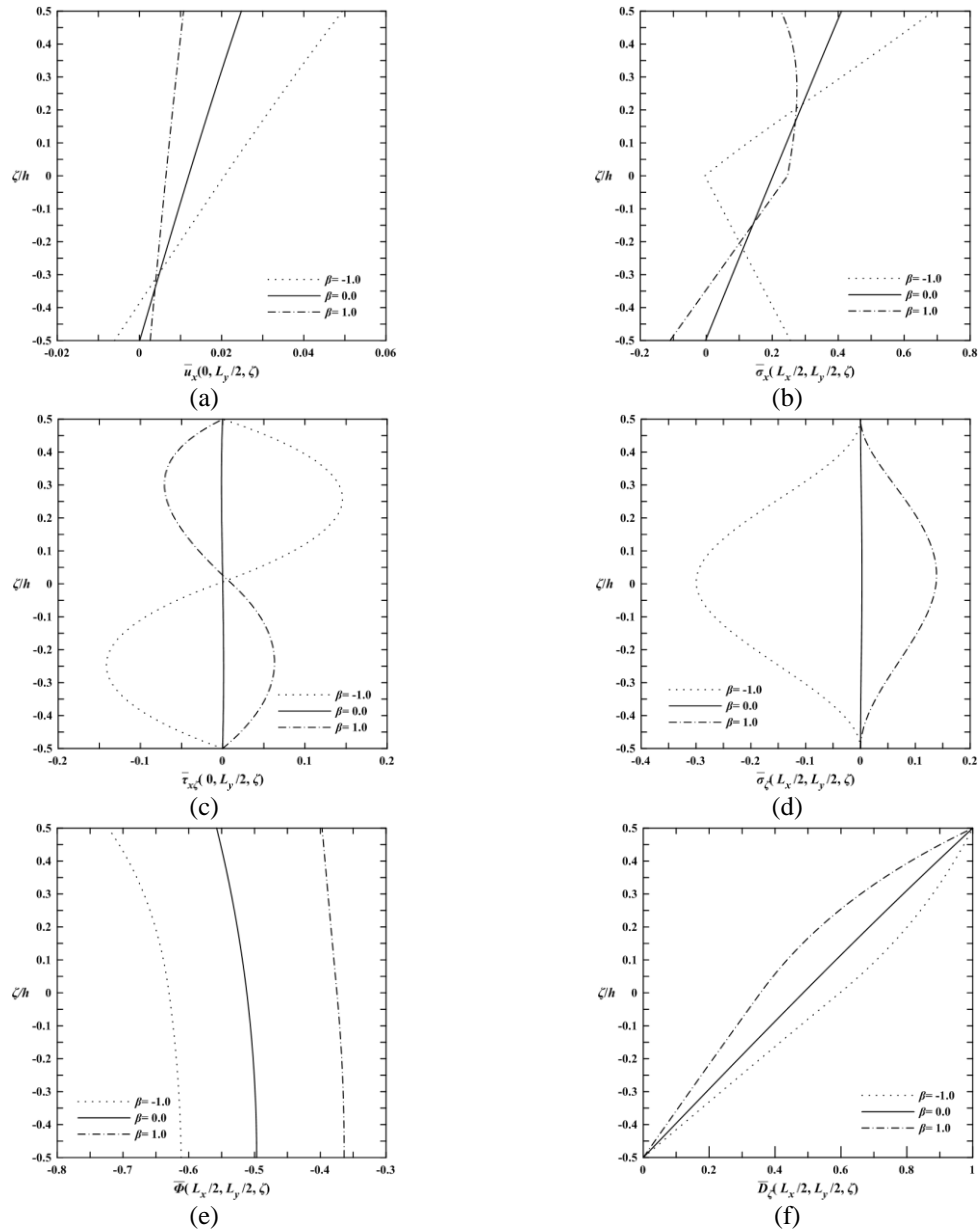

Fig. 5 The through-thickness distributions of various elastic and electric variables induced in an FGPM FSP for loading Case 2, in which β =-1.0, 0.0 and 1.0, $h_1 : h_2 = 0.5h : 0.5h$, and $L_x / h = 10$, $L_x = L_y$
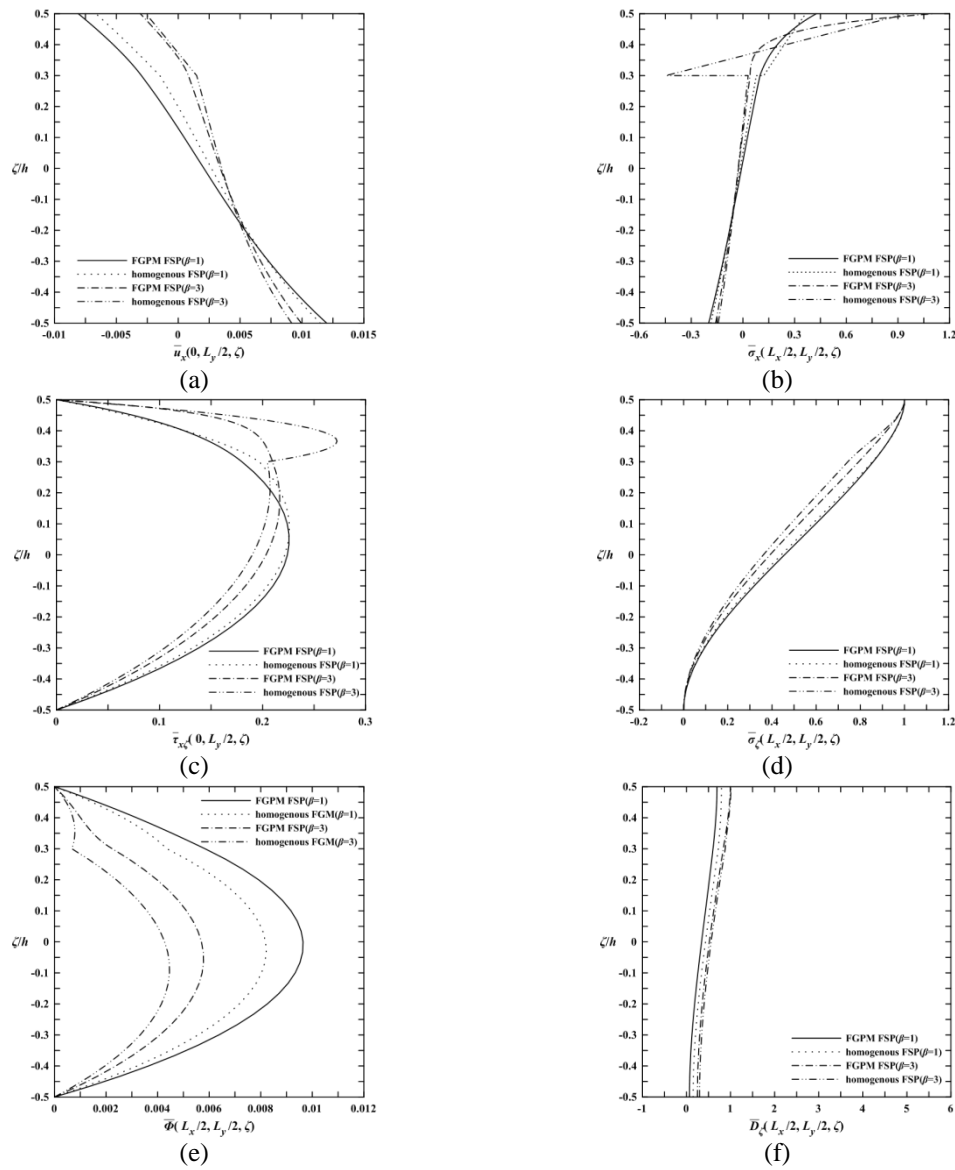
Fig. 6 The through-thickness distributions of various elastic and electric variables induced in an FGPM FSP for loading Case 3, in which β =-1.0, 0.0 and 1.0, $h_1 : h_2 = 0.5h : 0.5h$, and $L_x / h = 10$, $L_x = L_y$

The effects of different surface conditions (i.e., closed- and open-circuit ones) on the through-thickness distributions of elastic variables induced in the FGPM FSPs are very minor, while they are significant for those of electric variables. The results in Figs. 5 (Case 2) and 7 (Case

4) show the effects of different surface conditions on the through-thickness distributions of both electric and elastic variables are significant when the electric loads are applied.

(a)

(b)

(c)

(d)

(e)

(f)

Fig. 7 The through-thickness distributions of various elastic and electric variables induced in an FGPM FSP for loading Case 4, in which $\beta = -1.0$, 0.0 and 1.0, $h_1 : h_2 = 0.5h : 0.5h$, and $L_x / h = 10$, $L_x = L_y$
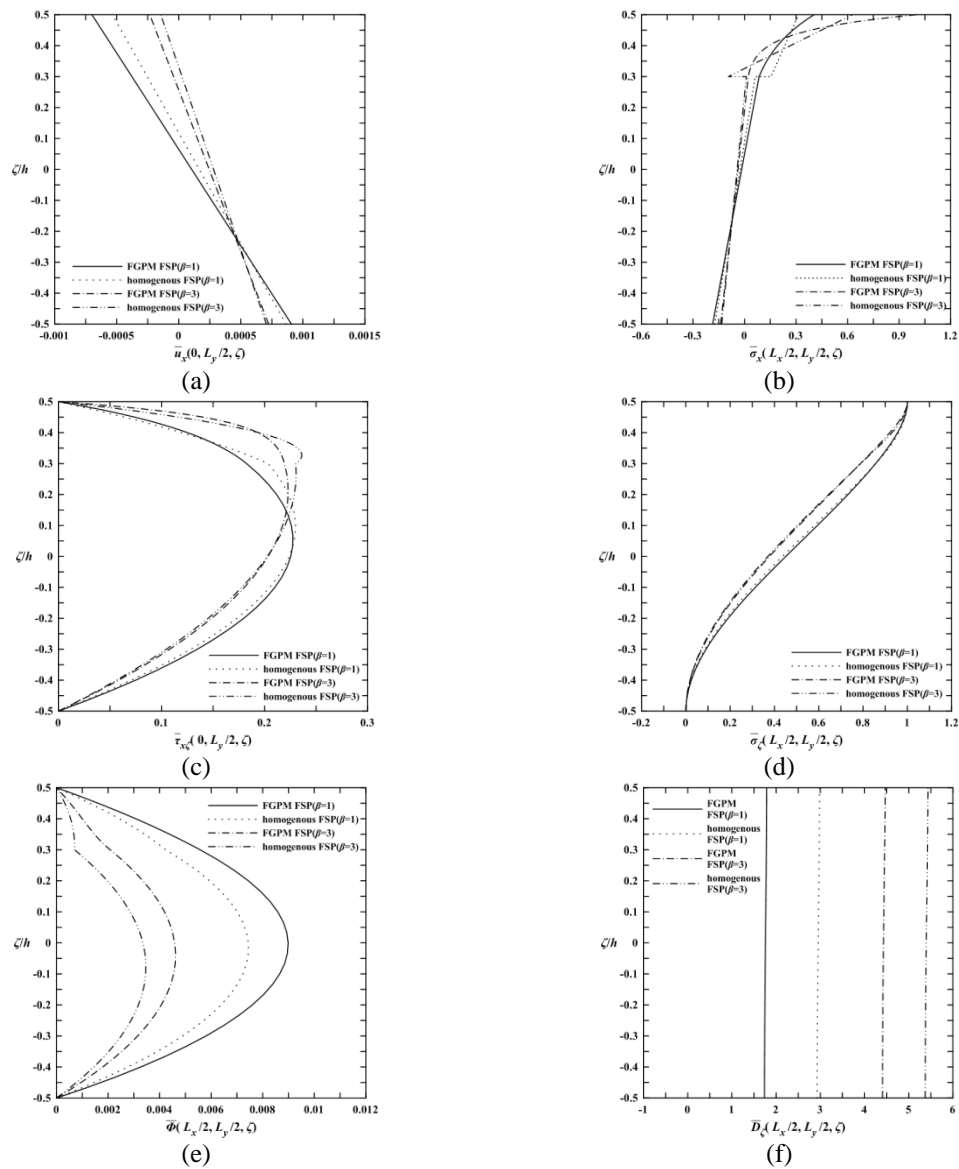
Fig. 8 The through-thickness distributions of various elastic and electric variables induced in an FGPM
FSP for loading Case 1, in which $\beta = 1.0$ and 3.0, $h_1 : h_2 = 0.8h : 0.2h$, and $L_x / h = 4$, $L_x = L_y$

   Figs. 8 and 9 show the through-thickness distributions of elastic and electric variables induced
in the FGPM FSPs and homogeneous ones with $L_x / h = 4$ and 50, respectively, for the loading
Case 1, in which $L_x = L_y$, $\beta = 1$ and 3, $h_1 : h_2 = 0.8h : 0.2h$, and $\bar{q}_\zeta^+ = q_0 \sin(\pi x / L_x) \sin(\pi y / L_y)$
and $\bar{q}_\zeta^- = 0$. The material properties distributions through the thickness coordinate of the FGPM
FSP are given in Eq. (36), while those of the homogenous FSP are layer-wise constants, which are

$m_{ij}^* e^{\beta}$ and m_{ij}^* for the film and substrate layers, respectively. It can be seen in Figs. 8(c) and 9(c) that the transverse shear stresses in the homogeneous FSPs change dramatically through the thickness coordinate when the deviations of the material properties between the film and substrate layer become greater (i.e., β becomes greater), while this situation will be reduced when we replace the homogeneous film with an FGPM film.

Fig. 9 The through-thickness distributions of various elastic and electric variables induced in an FGPM FSP for loading Case 1, in which $\beta = 1.0$ and 3.0, $h_1 : h_2 = 0.8h : 0.2h$, and $L_x / h = 50$, $L_x = L_y$

Figs. 8(b) and 9(b) show the in-plane stresses induced in the homogenous FSPs change abruptly at the film-substrate interface due to the mismatched material properties occurring at this location, while those induced in the FGPM FSPs vary smoothly through the thickness coordinate and are continuous at the film-substrate interface. The results in Figs. (8) and (9) also show that for a thick FSP the through-thickness distributions of elastic and electric variables appear to be layer-wise higher-order polynomials, while those for homogeneous FSP change more dramatically than those of FGPM FSP, and that the deviations of between these for homogeneous FSPs and FGPM FSPs increase when the material-property gradient (β) becomes greater.

4. Conclusions

In this article, we developed an RMVT-based FLM for the static analysis of simply-supported, FGPM FSPs with closed- and open-circuit surface conditions and subjected to four different loading conditions. The field variables are expanded as the trigonometric functions in the in-plane domains of the plate such that the simply-supported conditions are exactly satisfied, while these are interpolated in the thickness coordinate of each individual layer using Lagrange polynomials, the relevant orders of which can be freely selected to be linear, quadratic and cubic ones. In the implementation of various FLMs, the results show that $LM_{333}^{333} > LM_{222}^{222} > LM_{111}^{111}$, in which the symbol ">" means more accurate results and a more rapid convergence rate. In the numerical example, it is shown that the transverse shear stresses induced in the homogeneous FSPs change dramatically through the thickness coordinate when the deviations of the material properties between the film and substrate layers become greater, while this situation will be reduced when we replace the homogeneous film with an FGPM film. The in-plane stresses induced at the film-substrate interface for the homogeneous FSPs change abruptly due to the mismatched material properties occurring at that location, while those for the FGPM FSPs vary smoothly through the thickness coordinate of the plate and are continuous across the film-substrate interface. These advantages are helpful for overcoming some of the drawbacks of conventional homogeneous FSPs in practical applications, such as delamination and transverse matrix cracking. Moreover, the through-thickness distributions of electric and elastic variables induced in the FGPM FSPs and homogeneous ones appear to be layer-wise higher-order polynomial variations, which are inconsistent with the kinematic and kinetic assumptions of most of conventional two-dimensional (2D) equivalent-single-layered (ESL) theories of elastic plates. These 2D ESL theories of elastic plates might not be extended to those of FGPM FSPs, and some more advanced 2D theories of FGPM FSPs thus need to be developed.

Acknowledgments

References

Arefi, M. (2014), "Generalized shear deformation theory for the thermo elastic analyses of the functionally graded cylindrical shells", *Struct. Eng. Mech.*, **50**(3), 403-417.

Arefi, M., Rahimi, G.H. (2014), "Application of shear deformation theory for two dimensional electro-elastic analysis of a FGP cylinder", *Smart Struct. Syst.*, **13**(1), 1-24.

Arefi, M., Rahimi, G.H. and Khoshgoftar, M.J. (2012), "Exact solution of a thick walled functionally graded piezoelectric cylinder under mechanical, thermal and electric loads in the magnetic field", *Smart Struct. Syst.*, **9**(5), 427-439.

Ballhause, D., D'Ottavio, M., Kröplin, B. and Carrera, E. (2005), "A unified formulation to assess multilayered theories for piezoelectric plates", *Comput. Struct.*, **83**(15-16), 1217-1235.

Brischetto, S. and Carrera, E. (2010), "Advanced mixed theories for bending analysis of functionally graded plates", *Comput. Struct.* **88**(23-24), 1474-1483.

Brischetto, S. and Carrera, E. (2009), "Refined 2D models for the analysis of functionally graded piezoelectric plates", *J. Intell. Mat. Syst. Str.*, **20**, 1783-1797.

Brischetto, S. and Carrera, E. (2012), "Coupled thermo-electro-mechanical analysis of smart plates embedding composite and piezoelectric layers", *J. Therm. Stresses*, **35**(9), 766-804.

Carrera, E. (2003), "Theories and finite elements for multilayered plates and shells: a unified compact formulation with numerical assessment and benchmarking", *Arch. Comput. Method. E.*, **10**(3), 215-296.

Carrera, E. and Boscolo, M. (2007), "Classical and mixed finite elements for static and dynamic analysis of piezoelectric plates", *Int. J. Numer. Meth. Eng.*, **70**(10), 1135-1181.

Carrera, E., Brischetto, S. and Robaldo, A. (2008), "Variable kinematic model for the analysis of functionally graded material plates", *AIAA J.*, **46**(1), 194-203.

Carrera, E., Büttner, A. and Nali, P. (2010), "Mixed elements for the analysis of anisotropic multilayered piezoelectric plates", *J. Intell. Mat. Syst. Str.*, **21**(7), 701-717.

Kashtalyan, M. and Menshykova, M. (2009), "Three-dimensional elasticity solution for sandwich panels with a functionally graded core", *Compos. Struct.*, **87**(1), 36-43.

Liew, K.M., He, X.Q., Ng, T.Y. and Kitipornchai, S. (2003a), "Finite element piezothermoelasticity analysis and the active control of FGM plates with integrated piezoelectric sensors and actuators", *Comput. Mech.*, **31**(3), 350-358.

Liew, K.M., Sivashanker, S., He, X.Q. and Ng, T.Y. (2003b), "The modelling and design of smart structures using functionally graded materials and piezoelectric sensor/actuator patches", *Smart Mater. Struct.*, **12**(4), 647-655.

Loja, M.A.R., Mota Soares, C.M. and Barbosa, J.I. (2013), "Analysis of functionally graded sandwich plate structures with piezoelectric skins, using B-spline finite strip method", *Compos. Struct.*, **96**, 606-615.

Lu, P., Lee, H.P. and Lu, C. (2005), "An exact solution for functionally graded piezoelectric laminates in cylindrical bending", *Int. J. Mech. Sci.*, **47**(3), 437-438.

Lu, P., Lee, H.P. and Lu, C. (2006), "Exact solutions for simply supported functionally graded piezoelectric laminates by Stroh-like formalism", *Compos. Struct.*, **72**(3), 352-363.

Ootao, Y. and Ishihara, M. (2013), "Asymmetric transient thermal stress of a functionally graded hollow cylinder with piecewise power law", *Struct. Eng. Mech.*, **47**(3), 421-442.

Pan, E. (2003), "Exact solution for functionally graded anisotropic elastic composite laminates", *J. Compos. Mater.*, **37**(21), 1903-1920.

Pan, E. and Han, F. (2005), "Exact solution for functionally graded and layered magneto-electro-elastic plates", *Int. J. Eng. Sci.*, **43**(3-4), 321-339.

Reissner, E. (1984), "On a certain mixed variational theorem and a proposed application", *Int. J. Numer. Meth. Eng.*, **20**(7), 1366-1368.

Reissner, E. (1986), "On a mixed variational theorem and on a shear deformable plate theory", *Int. J. Numer. Meth. Eng.*, **23**(2), 193-198.

Saravanos, D.A. and Heyliger, P.R. (1999), "Mechanics and computational models for laminated piezoelectric beams, plates, and shells", *Appl. Mech. Rev.*, **52**(10), 305-320.

Sladek, J. Sladek, V., Stanak, P. and Pan, E. (2010), "The MLPG for bending of electroelastic plates", *CMES-Comput. Model. Eng. Sci.*, **64**, 267-297.

Sladek, J., Sladek, V., Stanak, P., Wen, P.H. and Atluri, S.N. (2012), "Laminated elastic plates with piezoelectric sensors and actuators", *CMES-Comput. Model. Eng. Sci.*, **85**, 543-572.

Sladek, J., Sladek, V., Stanak, P., Zhang, C. and Wunshe, M. (2013), "Analysis of bending of circular piezoelectric plates with functionally graded material properties by a MLPG method", *Eng. Struct.*, **47**, 81-89.

Tang, Y.Y., Noor, A.K. and Xu, K. (1996), "Assessment of computational models for thermoelectroelastic multilayered plates", *Comput. Struct.*, **61**(5), 915-933.

Tsai, Y.H. and Wu, C.P. (2008), "Dynamic responses of functionally graded magneto-electro-elastic shells with open-circuit surface conditions", *Int. J. Eng. Sci.*, **46**(9), 843-857.

Woodward, B. and Kashtalyan, M. (2010), "Bending response of sandwich panels with graded core: 3D elasticity analysis", *Mech. Adv. Mater. Struct.*, **17**(8), 586-594.

Wu, C.P. and Chang, Y.T. (2012), "A unified formulation of RMVT-based finite cylindrical layer methods for sandwich circular hollow cylinders with an embedded FGM layer", *Compos. Part B: Eng.*, **43**(8), 3318-3333.

Wu, C.P. and Li, H.Y. (2010a), "The RMVT- and PVD-based finite layer methods for the three-dimensional analysis of multilayered composite and FGM plates", *Compos. Struct.*, **92**(10), 2476-2496.

Wu, C.P. and Li, H.Y. (2010b), "RMVT- and PVD-based finite layer methods for the quasi-3D free vibration analysis of multilayered composite and FGM plates", *CMC-Comput. Mater. Continua*, **19**, 155-198.

Wu, C.P. and Li, H.Y. (2013a), "RMVT-based finite cylindrical prism methods for multilayered functionally graded circular hollow cylinders with various boundary conditions", *Compos. Struct.*, **100**, 592-608.

Wu, C.P. and Li, H.Y. (2013b), "An RMVT-based finite rectangular prism method for the 3D analysis of sandwich FGM plates with various boundary conditions", *CMC-Comput. Mater. Continua*, **34**, 27-62.

Wu, C.P. and Syu, Y.S. (2007), "Exact solutions of functionally graded piezoelectric shells under cylindrical bending", *Int. J. Solids Struct.*, **44**(20), 6450-6472.

Wu, C.P. and Tsai, Y.H. (2007), "Static behavior of functionally graded magneto-electro-elastic shells under electric displacement and magnetic flux", *Int. J. Eng. Sci.*, **45**(9), 744-769.

Wu, C.P. and Tsai, Y.H. (2009), "Cylindrical bending vibration of functionally graded piezoelectric shells using the method of perturbation", *J. Eng. Math.*, **63**(1), 95-119.

Wu, C.P., Chiu, K.H. and Wang, Y.M. (2008), "A review on the three-dimensional analytical approaches of multilayered and functionally graded piezoelectric plates and shells", *CMC-Comput. Mater. Continua*, **8**, 93-132.

Wu, C.P., Fan, T.Y. and Li, H.Y. (2014), "Reissner mixed variational theorem-based finite cylindrical layer methods for the 3D free vibration analysis of sandwich circular hollow cylinders with an embedded FGM layer", *J. Vib. Control*, **20**(8), 1199-1223.

Wu, X.H., Chen, C. and Shen, Y.P. (2002), "A high order theory for functionally graded piezoelectric shells", *Int. J. Solids Struct.*, **39**(20), 5325-5344.

Zhang, T., Shi, Z. (2010), "Exact analyses for two kinds of piezoelectric hollow cylinders with graded properties", *Smart Struct. Syst.*, **6**(8), 975-989.

Zhong, Z. and Shang, E.T. (2003), "Three-dimensional exact analysis of a simply supported functionally gradient piezoelectric plate", *Int. J. Solids Struct.*, **40**(20), 5335-5352.

Zhong, Z. and Yu, T. (2006), "Vibration of a simply supported functionally graded piezoelectric rectangular plate", *Smart Mater. Struct.*, **15**(5), 1404-1412.

CC